Ore Geology Reviews 84 (2017) 309–327

Contents lists available at ScienceDirect

Ore Geology Reviews

journal homepage: www.elsevier.com/locate/oregeo

Middle Devonian volcanic rocks in the Weibao Cu–Pb–Zn deposit, East Kunlun Mountains, NW China: Zircon chronology and tectonic implications

Shihua Zhong [a], Chengyou Feng [a,*], Reimar Seltmann [b], Daxin Li [a]

[a] MLR Key Laboratory of Metallogeny and Mineral Assessment, Institute of Mineral Resources, Chinese Academy of Geological Sciences, Beijing 100037, China
[b] Center for Russian and Central EurAsian Mineral Studies, Department of Earth Sciences, Natural History Museum, London SW7 5BD, UK

ARTICLE INFO

Article history:
Received 2 August 2016
Received in revised form 15 January 2017
Accepted 19 January 2017
Available online 21 January 2017

Keywords:
Geochronology
Post-collision
Skarn deposit
Weibao
Qimantagh
East Kunlun

ABSTRACT

The Weibao copper–lead–zinc deposit, located in the eastern part of the Qimantagh area, East Kunlun Orogenic Belt (EKOB), consists of three skarn ore blocks known as Weixi, Main and Weidong from west to east. The mineralization within the Weibao Cu–Pb–Zn deposit is hosted by the Mesoproterozoic Langyashan Formation. In this study, we describe for the first time basaltic lavas that intruded into this host sequence and chronological, isotopic, major and trace element data of these volcanic rocks are presented here to constrain their eruption age as well as the tectonic setting. Two basaltic lava samples yield sensitive, high-resolution ion-microprobe (SHRIMP) U–Pb zircon ages of 393.0 ± 5.5 Ma–392.0 ± 5.0 Ma, indicating that volcanic rocks in the Weibao deposit erupted in Middle Devonian. The majority of the volcanic rocks have compositions characterized by high potassium, light rare earth element (LREE)-enriched patterns in chondrite-normalized rare earth elements (REE) diagrams, and evident enrichment of Rb, Ba and K and depletion of Th, U, Nb and Ta contents in primitive mantle-normalized patterns, although the degrees of enrichment and depletion are variable. These characteristics of major and trace element data highlight a hornblende-dominated fractionation during ascent of magmas. The εHf(T) values of zircons are relatively scattered and slightly enriched, ranging from −2.6 to +7.5. Modelling the features of the major, trace and isotopic element data indicates a hybrid origin involving combined depleted mantle (and hence asthenospheric mantle) and melts and/or fluids inherited from an early subduction event. Besides, these geochronological and geochemical data, together with previously published data in the EKOB, suggest that the Weibao basaltic lavas formed in a post-collisional setting, and that the Qimantagh area underwent strong interactions between mantle and crust in Early Paleozoic–Middle Devonian.

1. Introduction

The East Kunlun Orogenic Belt (EKOB) is a long (about 1500 km) tectonic belt extending across central China and located in the Northern Qinghai–Tibet Plateau, bounded by the Qaidam Basin to the north, the Bayan Har–Songpan Ganzi block to the south, the Qinling–Dabie orogenic belt to the east and the NE–trending Altyn Tagh fault to the west (Mo et al., 2007; Xiong et al., 2012). It records a long and complex history of plate collision, tectonic deformation and magmatic activities, beginning in Early Paleozoic and continuing into Cenozoic (Yang et al., 1996; Mo et al., 2007; Jiang et al., 2009; Hao et al., 2015; and references therein). As a part of the EKOB, the Qimantagh area well recorded early stages of tectono-magmatic evolution processes of the EKOB, i.e., Early Paleozoic to Middle Devonian tectono-magmatic activities. However, due to unfavourable outcrop situation and particularly, the complex superimposed orogenic processes (Li, 2010; Hao et al., 2015), the evolution history of the Qimantagh area during the Early Paleozoic to Middle Devonian is still poorly understood.

The Weibao Cu–Pb–Zn deposit, initially discovered through geochemical reconnaissance survey by the Geophysical and Geochemical Party, Xinjiang Bureau of Geology and Mineral Resource Exploration and Development (GGPXBGMRXD) in 2003, is located at the boundary of Xinjiang and Qinghai, China (37°07′58″ N, 91°07′08″ E, Fig. 1b), and now has been one of the most promising skarn deposits in the Qimantagh area. Previous studies with regard to this deposit reported the characteristics of orebodies and fluid geochemistry (e.g., Gao et al., 2014c; Fang et al., 2015), whereas

* Corresponding author.
E-mail address: fengchy@cags.ac.cn (C. Feng).

http://dx.doi.org/10.1016/j.oregeorev.2017.01.020
0169-1368/

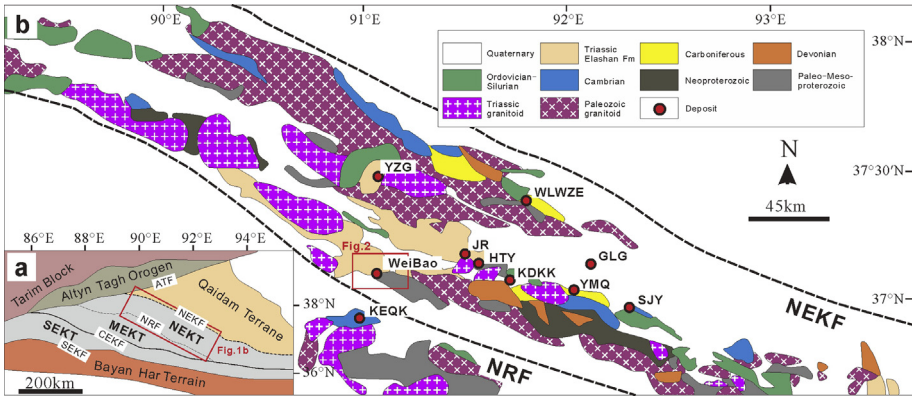

Fig. 1. a. Simplified geological map of the Qimantagh area (modified after Fang et al., 2015). b. Geological map of the North Qimantagh magmatic arc showing the locations of main skarn deposits (modified after Feng et al., 2011b; Fang et al., 2015). Abbreviations: NEKT–North East Kunlun terrane; MEKT–Middle East Kunlun terrane, SEKT–South East Kunlun terrane, ATF–Altyn Tagh fault, NEKF–North East Kunlun fault, NRF–Nalingguole River fault, CEKF–Central East Kunlun fault, SEKF–South East Kunlun fault. The names of skarn deposits are: KEQK–Kaerqueka, YZG–Yazigou, JR–Jingren, HTY–Hutouya, KDKK–Kendekeke, WLWZE–Wulanwuzhuer, YMQ–Yemaquan, GLG–Galinge, SJY–Sijiaoyang.

few have focused on igneous activities in this area. As a result of our recent work and detailed investigations, for the first time volcanic rocks intruded into the host sequence of the Weibao deposit were found, marking the occurrence of volcanic eruption in the Weibao deposit.

We collected fresh lava samples from the Weibao deposit and a systematic research on geochronology and geochemistry of these rocks was conducted in order to constrain the eruption time, the tectonic setting and the magmatic source of those volcanic rocks, whereas the nature of the deposit itself in terms of mineralization, alteration, and veining styles for example, is only roughly described as it is not the focus of this paper. Additionally, combined with previously published age data, a new combined petrologic and tectonic model is proposed aiming to better understand the evolution history of the Early Paleozoic– Devonian tectono-magmatic cycle within the Qimantagh area.

2. Geological setting

2.1. Regional setting

The EKOB is subdivided by the Nalingguole River fault (NRF) and the Central East Kunlun fault (CEKF) into three distinct zones from north to south, referred to as the North East Kunlun terrain (NEKT), the Middle East Kunlun terrain (MEKT) and the South East Kunlun terrain (SEKT) respectively (Fig. 1a). Generally, it consists of four orogenic cycles over several eras, i.e., the Precambrian, the Early Paleozoic Caledonian, the Late Paleozoic–Early Mesozoic Hercynian–Indosinian and the Late Mesozoic–Cenozoic Yanshan–Himalaya cycles, respectively (e.g., Liu et al., 2005; Mo et al., 2007; Hao et al., 2015). A thorough regional review of lithological, geochemical, structural, metamorphic and geochronological characteristics of the EKOB, as well as the tectono-magmatic evolution histories with regard to these four cycles, has been summarized by Mo et al. (2007) and is therefore not repeated here.

The Qimantagh area, situated within the western part of the EKOB, is a wedge field among the Altyn Tagh Orogen, Qaidam Basin and Bayan Har terrain, bounded by the ATF, SEKF and NEKF, respectively (Fig. 1a) (Fang et al., 2015). Generally, it can be subdivided into three tectonic units from north to south (Gao et al., 2010): (1) the Early Paleozoic North Qimantagh magmatic arc, i.e., the western part of NEKT (Fig. 1b), (2) the Central Kunlun massif, i.e., the western part of MEKT, and (3) the Early Paleozoic accretionary wedge, i.e., the western part of SEKT.

The rocks of different ages, ranging from Archean to Cenozoic, widely occur within the Qimantagh area (Fig. 1b). The basement rocks are mainly composed of the Jinshuikou, Xiaomiao, and Binggou Groups (Liu et al., 2005), which are Archean to Proterozoic in age. The Langyashan Formation and Qimantagh Group (also known as the Tanjianshan Goup), as well as the Carboniferous strata, are the most important host rocks for the skarn mineralization within the Qimantagh area (e.g., Feng et al., 2011b). The Langyashan Formation is described as Mesoproterozoic in age and consists of the carbonate rocks and clastic rocks, locally undergoing greenschist facies metamorphism (Xu et al., 2012). In contrast, the Qimantagh Group is known as Ordovician–Silurian in age and comprises volcano-sedimentary rocks, but also experienced greenschist facies metamorphism (e.g., Wang et al., 2003; Li et al., 2007).

Published descriptions of the structural setting of the Qimantagh area indicate the presence of faults and folds (Feng et al., 2010, 2012; Gao et al., 2010). The fold orientations mostly trend from west–northwest to east–southeast, whereas the fault systems are more complicated. The faults striking west–northwest, northwest and east are interpreted to be produced before and/or during the skarn mineralization, therefore usually controlling significant mineralization. The northeast- and north-striking fault systems are generally post-skarn and post-mineralization, but likely control the emplacement of post-skarn intrusions. Besides, the earlier fault systems are likely reactivated by subsequent tectonic activities. Abundant intrusions of different ages are preserved in the Qimantagh area (Fig. 1b). Both of the Paleozoic and Triassic granitoids are volumetrically widespread (Wang et al., 2009; Feng et al., 2010, 2012; Gao and Li, 2011; Gao et al., 2012a, 2012b, 2014a, 2014b; Li et al., 2012; Xiao et al., 2013), whereas economic Cu–Pb–Zn–Fe mineralization is mainly related to Triassic granitoids (e.g., Feng et al., 2009, 2010, 2011a, 2012). Other igneous rocks, such as mafic dykes, are mainly post-skarn and post-mineralization (e.g., Luo et al., 2002).

2.2. Geology of the Weibao cu–pb–zn deposit

The Weibao Cu–Pb–Zn deposit occurs at an elevation of ca. 5000 m asl in the EKOB and is one of several in the Qimantagh Cu–Zn–Pb–Fe belt, a Phanerozoic metallogenic belt of igneous rocks which extends for ca. 550 km in NW–SE direction (Fig. 1b) (Feng et al., 2010; Zhao et al., 2013). It comprises the Weixi ore block to the west, the Main ore block to the centre and the Weidong ore block to the east (Fig. 2) which are mainly characterized by Cu, Cu–Pb–Zn and Pb–Zn mineralization respectively, whereas

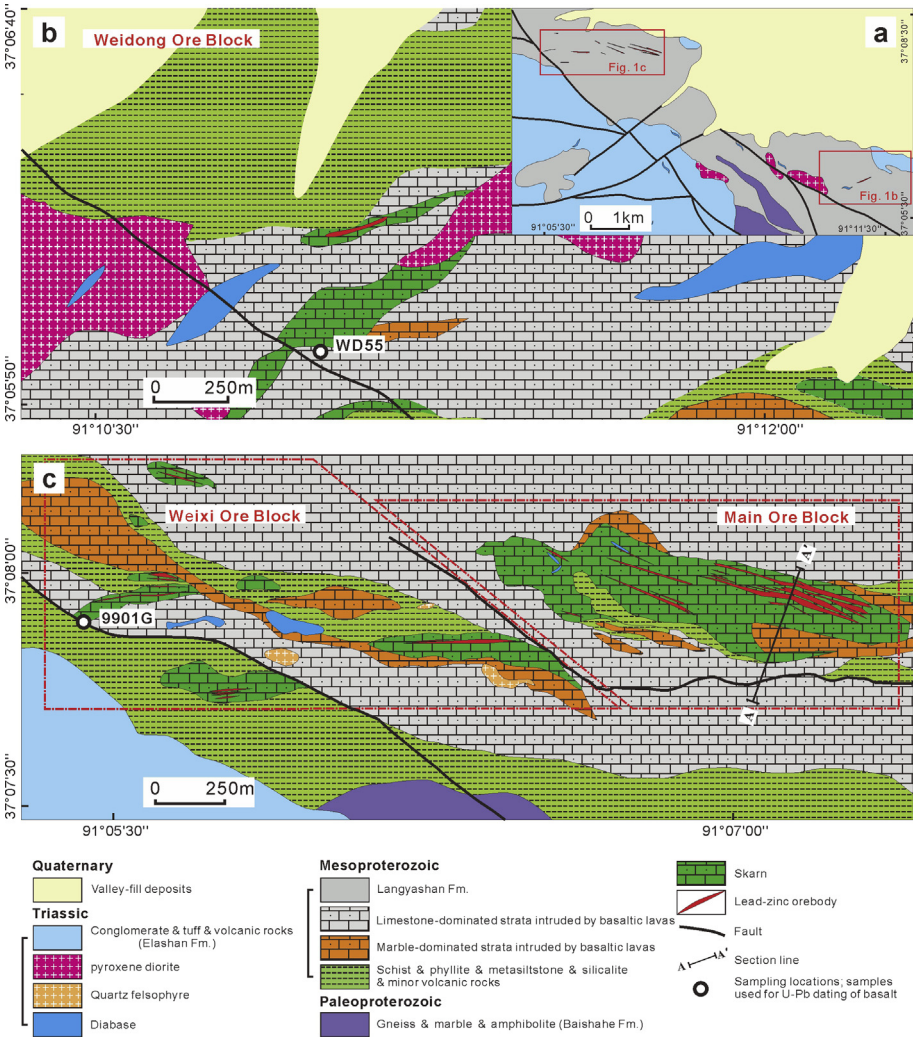

Fig. 2. a. Simplified geological map of the Weibao Cu–Pb–Zn deposit showing the locations of the Weidong, Main and Weixi ore blocks. b. Geological map of the Weidong ore block. c. Geological map of the Weixi and Main ore blocks. All these figures are modified after unpublished maps from GGPXBGMRXD. Note that the Middle Devonian basaltic lavas are identified for the first time in this study and are widespread in the Weibao district, but currently there are not enough geological data to recompile the map of this poor studied district.

minor Cu mineralization also occurs in the Weidong ore block (Fig. 2b). Geographically, the Weixi and Main ore blocks are subdivided by a northeast-striking fault (Fig. 2c). Although Cu mineralization is especially predominant in the Weixi ore block, there is no economic Cu orebody occurring at the surface (Fig. 2c). Currently, a precise temporal constraint is absent within the Weibao deposit, but it is reasonable to assume that the main Cu–Pb–Zn mineralization was emplaced during Middle and Late Triassic, in view of the consistent Middle to Late Triassic mineralization ages obtained from other skarn deposits in the Qimantagh metallogenic belt (e.g., Li et al., 2008; Feng et al., 2009, 2011a; Yu et al., 2015) with the exception of the Baiganhu deposit (Zhou et al., 2015).

Regardless of the distinction with respect to the mineralization, the orebodies in the Weibao deposit are hosted by the same rock unit (known as the Langyashan Formation) that exposes variable degrees of metamorphism (Li, 2010; Gao et al., 2014c). This sequence reaches a thickness of nearly 1.5 km and consists predominantly of limestone, marble, skarn, pyroclastic rocks and minor siltstone (Fig. 3). Spatially, these rocks are unconformably overlain by the Triassic Elashan Formation and underlain by the Paleoproterozoic Baishahe Formation. The Elashan Formation is mainly composed of andesite, dacite, rhyolite and pyroclastic rocks, whereas the Baishahe Formation dominantly consists of gneiss, marble and amphibolite manifesting amphibolite and granulite facies metamorphism. Both the Elashan and Baishahe Formations are nonreactive and do not host significant skarn mineralization. On the basis of detailed field observations, core logging and thin section petrography, we found for the first time basaltic lavas (basalts and minor basaltic andesites) that intruded into the host sequence in the Weibao deposit (Fig. 4a, b). These lavas preserve amygdaloidal and/or porphyritic volcanic structures (Fig. 4c, d, e, f) that make them noticeably different from other rock types in this area. Locally, these lavas suffered strong alteration and metamorphism, resulting in invisibility of those volcanic structures.

The granodiorite are widespread in the Weibao district but might be unrelated to alteration and mineralization by virtue of their space relationships. Undated monzonite porphyry with minor Pb–Zn mineralization is found in the drill holes of both the Weixi and Weidong ore blocks, indicating that alteration and mineralization might genetically associate with them. Other igneous rocks, such as mafic dykes, pyroxene diorite, rhyolite and porphyritic granite, also occur within the Weibao deposit. Our unpublished chronological data show that these intrusions mainly formed in

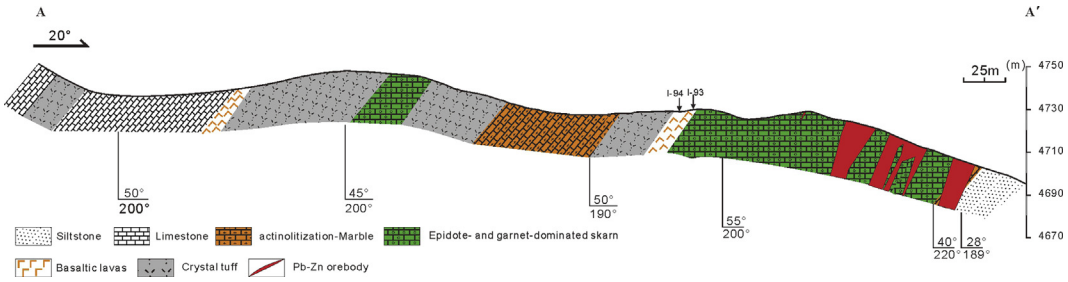

Fig. 3. Geological cross section along A–A′ in Fig. 2c. Note that the locations of two volcanic rock samples (samples I-93 and I-94) from the Main ore block are shown.

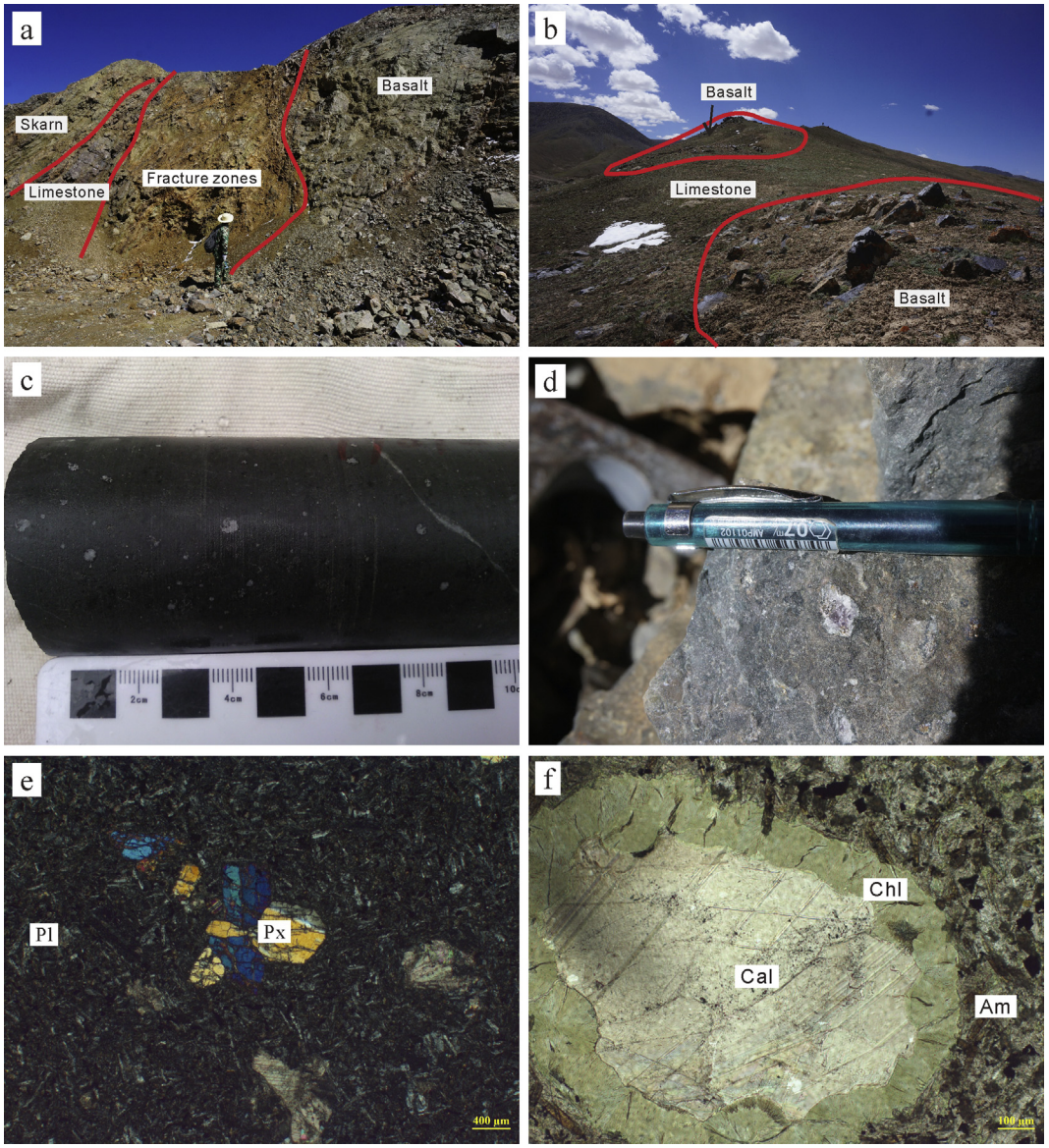

Fig. 4. Photographs of basaltic lavas from the Weibao deposit. a. Basaltic lavas intruded into limestone in the Weixi ore block, with a fracture between their contact zone. b. Outcrops of basaltic lavas in the Weidong ore block. c. Hand-sized specimen showing an amygdaloidal structure. d. Amygdales filled with fluorite. e. Porphyritic basalts showing phenocrysts of pyroxene (cross-polarized light). f. Amygdales consisting of carbonate in the core and chlorite in the rim (plane-polarized light).

Lower Triassic (232–227 Ma), but minor formed in Early Devonian (~408 Ma). Further investigation is needed to clearly illustrate the temporal and spatial relationships between these igneous rocks and mineralization.

3. Sample description and analytical methods

3.1. Sample description

Lavas from the Weibao deposit are dark gray to black in color and mostly preserve primary igneous textures, e.g., vesicular and amygdaloidal structures (Fig. 4c, d, f). Typical amygdales are composed of carbonate in the core and chlorite in the rim (Fig. 4f), and others consist of carbonate or chlorite or fluorite (Fig. 4d). Since the majority of lavas occurring within the Weibao deposit underwent variable degrees of deformation and metamorphism, the utmost care was required in the selection and treatment to reduce the influence introduced by these processes. Seven least altered lava samples without evident vesicular and amygdaloidal structures were analyzed in this study and detailed descriptions were given in Table 1. These rocks are, in general, basaltic and/or basaltic–andesitic in composition. The mineralogical assemblages of these samples exhibit olivine, clinopyroxene, amphibole, plagioclase, K-feldspar and magnetite. Texturally, they are generally porphyritic (Fig. 4c) but in some cases they are granular. The groundmass of these volcanic rocks is mainly composed of holocrystalline to coarsely microcrystalline plagioclase, pyroxene and Fe–Ti oxides, and is commonly overprinted by intergrowths of albite, actinolite and epidote with minor oxide, carbonate and chlorite. The phenocrysts are predominantly composed of olivine, clinopyroxene and amphibole with minor K-feldspar. Most of K-feldspar within these lavas are secondary and introduced by local potassic alteration. The phenocrysts of plagioclase are either locally albitised or replaced by an aggregate of microcrystalline epidote, calcite and chlorite, whereas the pyroxene is typically replaced by ragged actinolite–albite–epidote–chlorite–calcite intergrowths. These alteration assemblages match well with metamorphism of rocks to lower greenschist facies (e.g., Squire et al., 2006; Watchorn and Wilson, 1989).

3.2. Analytical methods

Zircons were separated from samples 9901G (37°07′55″ N, 91°05′22″ E; Fig. 2c) and WD55 (37°05′56″ N, 91°11′03″ E; Fig. 2b) using magnetic and heavy liquid separation. Approximately 150 zircon grains from each sample were mounted and polished in 25-mm epoxy discs. The internal zoning patterns of the crystals were observed by cathodoluminescence (CL) image analysis at the Institute of Mineral Resources, Chinese Academy of Geological Sciences (CAGS). Zircon was then analyzed for U–Th–Pb isotopic dating by high-resolution ion microprobe (SHRIMP II) at the SHRIMP Laboratory in Beijing SHRIMP Centre, CAGS. Instrumental conditions and measurement procedures were similar to those described by Compston et al. (1992). Spots of approximately 30-μm diameter were analyzed; seven scans through the critical mass range were used for data collection. The U and Th contents were calibrated using reference zircon of SL13 from Sri Lanka (U = 238 ppm; $^{206}Pb/^{238}U = 0.0928$; 572 Ma; Liu et al., 2004; Wan et al., 2006). Repeated analyses of the standard during the analytical session were used to determine concentrations of U, Th and Pb and to calibrate the inter-element isotopic ratios of the samples. Data processing was carried out using the Squid and Isoplot programs (Lugwig, 2001) and the measured ^{204}Pb was used for the correction of common lead. The errors given in Table 2 for individual analyses are quoted at the 1σ level, whereas the errors for weighted mean ages given in Fig. 6, and in the text, are quoted at 2σ (95% confidence level).

Seven samples were collected for major and trace element analyses and measured at the National Research Centre of Geoanalysis, CAGS. They were trimmed to remove weathered surfaces, cleaned with deionized water, crushed and then powdered to 200-mesh using an agate mill. Major oxides were analyzed by a SHIMADZU MRF-2100 X-ray Fluorescence Spectrometry (XRF), with FeO and loss–on–ignition (LOI) analyzed by wet chemical methods. Analytical uncertainties were better

Table 1
Descriptions of samples from the Weibao deposit.

Sample No.		Location	Coordinate	Texture	Mineral components	Alteration
9901–6–1	Basalt	WX	E91°05′21.83″ N37°07′50.14″	Porphyritic texture	Phenocrysts: plagioclase (30%), augite (10%) and olivine (5%); Matrix(50% ca.): microlites of plagioclase, clinopyroxene, minor olivine, minor magnetite, and minor ilmenite	Minor pyroxene is replaced by actinolite–albite–epidote–chlorite–calcite intergrowths; plagioclase is replaced by albite and K-feldspar
9901–6–2	Basalt		E91°05′21.83″ N37°07′50.14″	Porphyritic texture	Phenocrysts: plagioclase (25%), clinopyroxene (10%) and brown hornblende (10%); Matrix(50% ca.): microlites of plagioclase, clinopyroxene, minor magnetite, and minor ilmenite	Groundmass is overprinted by intergrowths of albite and epidote with minor hematite, carbonate and chlorite; minor K-feldspar occurs as secondary stockworks
9901–7	Basalt		E91°05′21.83″ N37°07′50.14″	Granular texture	Plagioclase (60% ca.), clinopyroxene (15%), olivine (5%), magnetite (15%) and minor ilmenite granules	Minor pyroxene is replaced by actinolite, epidote and chlorite; minor plagioclase is replaced by microcrystalline epidote, calcite and chlorite; K-feldspar occurs as secondary stockworks
I–93	Basaltic andesite	M	E91°07′7.26″ N37°07′55.50″	Porphyritic texture	Phenocrysts: plagioclase (40%), brown hornblende (10%), and orthopyroxene (5%). Matrix (40% ca.): cryptocrystalline mass crowded with plagioclase microlites and magnetite granules	Plagioclase is replaced by albite and epidote; minor K-feldspar occurs as secondary stockworks
I–94	Basalt		E91°07′7.08″ N37°07′54.42″	Granular texture	Plagioclase (60% ca.), clinopyroxene (15%), brown hornblende (5%), magnetite (15%) and minor ilmenite granules	Plagioclase is replaced by albite and epidote; Minor pyroxene is replaced by actinolite–albite–epidote–chlorite–calcite intergrowths
WD–104	Basalt	WD	E91°10′56.02″ N37°06′12.26″	Granular texture	Plagioclase (65% ca.), clinopyroxene (15%), brown hornblende (5%) and magnetite (15%) granules	Minor chlorite and calcite replacing pyroxene
WD55	Basaltic andesite		E91°11′02.58″ N37°05′55.62″	Porphyritic texture	Phenocrysts: plagioclase (35% ca.), brown hornblende (10%), and orthopyroxene (5%). Matrix (55% ca.): plagioclase, hornblende, orthopyroxene and magnetite	Plagioclase is replaced by albite and epidote; minor K-feldspar occurs as secondary stockworks

Abbreviations: WX, Weixi ore block; M, Main ore block; WD, Weidong ore block.

Table 2
SHRIMP zircon analyses of basaltic lavas from the Weibao deposit.

Spot	$^{206}Pb_c$/%	U/ppm	Th/ppm	Th/U	$^{206}Pb*$/ppm	$^{206}Pb/^{238}U$ Age (Ma)	1σ	$^{207}Pb/^{206}Pb$ Age (Ma)	1σ	$^{208}Pb/^{232}Th$ Age (Ma)	1σ	$^{207}Pb*/^{206}Pb*$	%	$^{207}Pb*/^{235}U$	%	$^{206}Pb*/^{238}U$	%
Weixi																	
9901G-1	0.00	983	410	0.42	52.7	390.7	3.6	378.1	29	387.7	6	0.0542	1.3	0.467	1.6	0.0625	0.9
9901G-2	−0.03	962	65	0.07	51.8	392.0	8.9	357.4	27	382.9	16	0.0537	1.2	0.464	2.6	0.0627	2.3
9901G-3	0.08	269	170	0.63	14.9	401.5	9.3	456.2	50	394.9	12	0.0561	2.3	0.497	3.3	0.0643	2.4
9901G-4	0.12	493	283	0.57	27.1	399.2	9.1	371.5	40	391.4	11	0.0540	1.8	0.476	3.0	0.0639	2.4
9901G-5	0.05	599	116	0.19	97.6	1119.3	24.0	1975.8	11	2058.3	51	0.1213	0.6	3.172	2.4	0.1896	2.3
9901G-6	0.23	216	117	0.54	47.4	1463.0	31.3	1544.1	20	1395.3	39	0.0958	1.1	3.366	2.6	0.2548	2.4
9901G-7	0.58	344	126	0.37	18.9	397.7	9.2	400.7	96	377.3	22	0.0547	4.3	0.480	4.9	0.0636	2.4
9901G-8	1.43	94	98	1.04	12.6	920.6	22.1	1115.4	137	1076.7	62	0.0768	6.9	1.625	7.3	0.1535	2.6
9901G-9	0.30	874	361	0.41	46.0	382.4	6.0	317.0	47	353.3	10	0.0527	2.0	0.444	2.6	0.0611	1.6
9901G-10	0.66	563	260	0.46	30.8	394.7	6.8	248.2	86	346.2	14	0.0512	3.8	0.445	4.2	0.0631	1.8
9901G-11	0.27	995	64	0.06	53.1	387.8	6.4	355.7	59	311.1	62	0.0536	2.6	0.458	3.1	0.0620	1.7
9901G-12	0.26	324	222	0.69	17.9	400.3	7.1	480.3	114	376.8	15	0.0567	5.2	0.501	5.5	0.0641	1.8
9901G-13	1.30	267	160	0.60	15.1	406.3	7.5	285.5	124	359.0	15	0.0520	5.4	0.466	5.8	0.0651	1.9
9901G-14	0.43	732	56	0.08	38.5	380.9	6.4	413.2	79	469.7	70	0.0550	3.5	0.462	3.9	0.0609	1.7
Weidong																	
WD55-1	0.34	689	284	0.41	36.9	387.9	3.7	274.0	33	353.2	6	0.0517	1.4	0.442	1.7	.0620	1.0
WD55-2	0.14	2711	1056	0.39	149.7	401.2	9.0	363.5	20	391.1	10	0.0538	0.9	0.476	2.5	0.0642	2.3
WD55-3	−0.05	201.90	132.93	0.66	28.04	966.6	21.5	1015.6	26	954.8	25	0.0731	1.3	1.630	2.7	0.1618	2.4
WD55-4	0.18	988	522	0.53	52.1	383.6	8.7	365.6	30	364.6	9	0.0539	1.4	0.455	2.7	0.0613	2.3
WD55-5	0.36	241	118	0.49	12.7	383.2	9.0	279.8	78	375.8	14	0.0519	3.4	0.438	4.2	0.0613	2.4
WD55-6	0.64	142.47	175.82	1.23	22.74	1092.1	24.6	1011.5	56	1061.1	31	0.0729	2.8	1.856	3.7	0.1846	2.4
WD55-7	1.54	426	152	0.36	22.2	374.1	8.7	506.3	174	370.1	34	0.0574	7.9	0.473	8.3	0.0597	2.4
WD55-8	0.10	180	114	0.63	9.7	393.3	9.4	354.9	124	387.5	18	0.0536	5.5	0.465	6.0	0.0629	2.5
WD55-9	0.02	3783	1661	0.44	213.5	410.1	9.2	390.2	13	403.1	10	0.0545	0.6	0.493	2.4	0.0657	2.3
WD55-10	0.30	512	298	0.58	27.8	394.2	6.1	467.0	55	375.2	10	0.0564	2.5	0.490	3.0	0.0631	1.6
WD55-11	0.08	3830	1687	0.44	215.4	408.4	5.9	376.5	16	393.8	7	0.0541	0.7	0.488	1.7	0.0654	1.5
WD55-12	0.54	192	122	0.63	10.5	395.1	7.0	447.7	171	409.3	22	0.0559	7.7	0.487	7.9	0.0632	1.8
WD55-13	1.27	111	49	0.44	6.0	387.7	7.5	259.2	215	391.7	29	0.0514	9.3	0.439	9.6	0.0620	2.0
WD55-14	0.36	583	345	0.59	32.2	400.2	6.2	369.6	56	374.5	10	0.0540	2.5	0.477	2.9	0.0640	1.6
WD55-15	1.23	333	153	0.46	18.1	390.8	6.9	175.9	254	362.4	35	0.0496	10.9	0.427	11.0	0.0625	1.8

Note: $^{206}Pb_c$ (%) represents the percentage of common ^{206}Pb in total ^{206}Pb; *denotes radioactivity lead; common Pb corrected using measured ^{204}Pb.

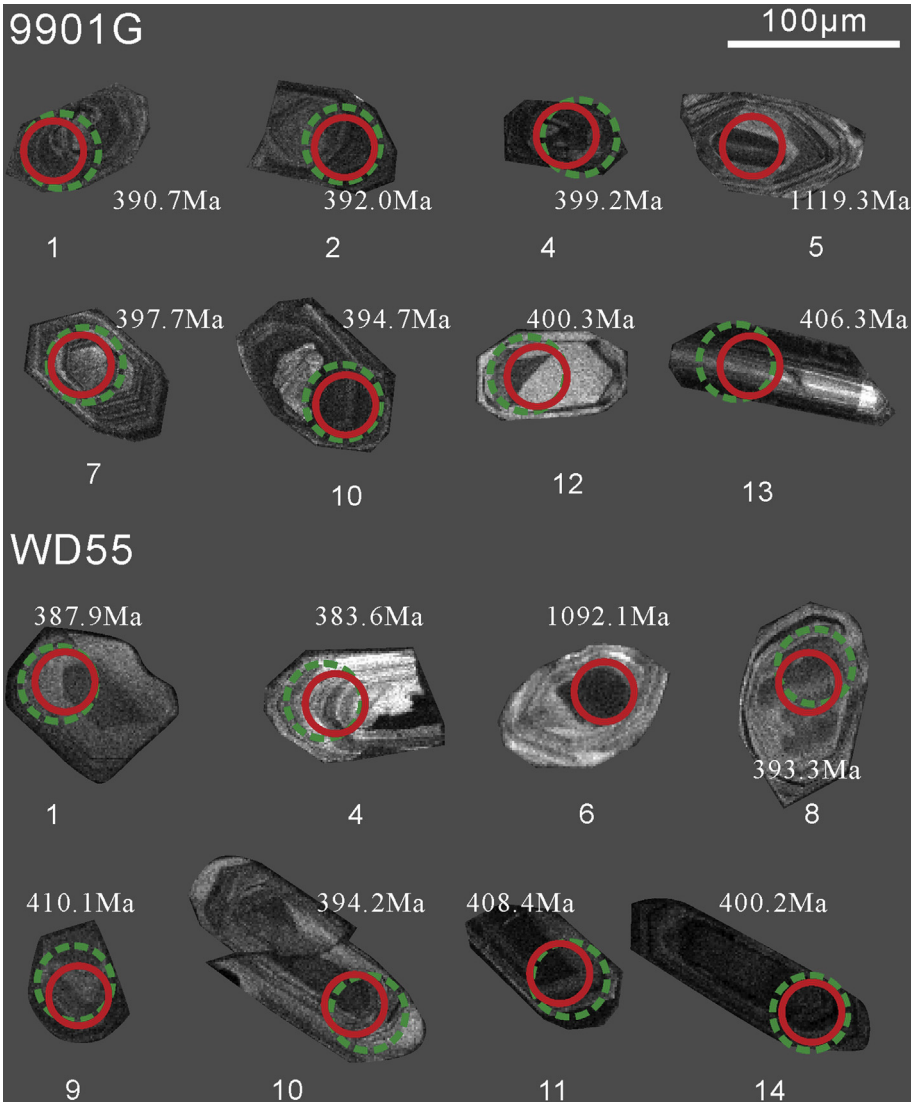

Fig. 5. CL images of zircons from basaltic lavas of the Weixi (sample 9901G) and the Weidong (sample WD55) ore blocks respectively. The locations for U–Pb (full circles) and Lu–Hf analyses (dotted circles) are shown.

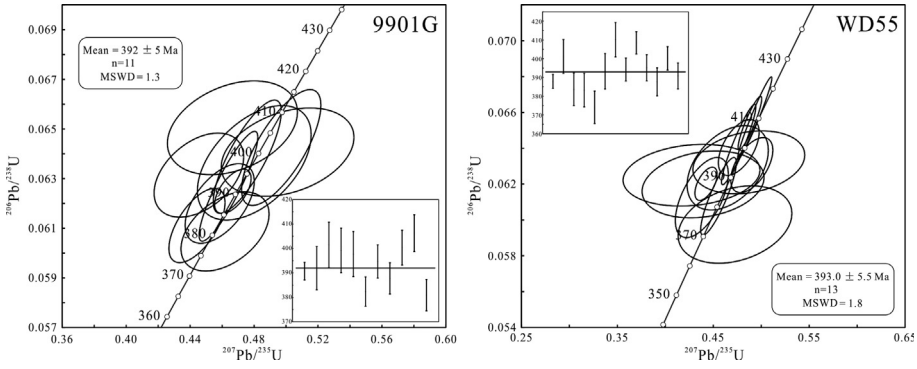

Fig. 6. SHRIMP Zircon U–Pb analyses for the basaltic lavas from the Weixi (sample 9901G) and the Weidong (sample WD55) ore blocks respectively.

than 0.5% for all major elements. Trace elements were analyzed by inductively coupled plasma mass spectrometry (ICP–MS) using PE300D. Detailed analytical procedures were similar to those described by Liu et al. (2016). Analyzed uncertainties of ICP–MS data at the ppm level were better than 5%.

In situ zircon Hf isotopic analysis was conducted on the same zircon grains that were previously analyzed for U–Pb dating, using a Neptune MC–ICP–MS coupled to a GeoLas UP193 laser ablation microprobe with a beam size of 44 μm and a laser pulse frequency of 8–10 Hz at the State Key Laboratory of Continental Tectonics and

Table 3
Major, trace and rare earth element concentrations of the lavas from the Weibao deposit.

Location	WX			M		WD	
Sample	9901-6-1 Basalt	9901-6-2 Basalt	9901-7 Basalt	I-93 Basaltic andesite	I-94 Basalt	WD-104 Basalt	WD55 Basaltic andesite
SiO_2 (wt%)	47.62	50.77	46.45	53.29	49.49	48.56	55.75
TiO_2	1.54	1.28	1.43	1.61	2.15	1.94	0.96
Al_2O_3	15.45	13.32	14.59	14.06	14.04	14.18	15.39
$Fe_2O_3^T$	8.85	13.65	8.71	10.54	12.43	13.96	7.78
FeO	5.21	5.36	5.23	7.71	8.34	9.28	4.66
MnO	0.15	0.14	0.17	0.15	0.12	0.21	0.13
MgO	6.52	6.52	7.52	4.55	5.74	5.22	3.71
CaO	6.11	6.47	7.87	7.24	6.66	9.88	4.66
Na_2O	1.50	1.96	2.13	3.89	3.49	2.77	3.53
K_2O	6.18	4.94	4.13	2.73	2.70	0.20	3.80
P_2O_5	0.47	0.46	0.40	0.16	0.16	0.17	0.33
LOI	4.81	5.39	5.48	1.07	1.79	2.53	3.25
La (ppm)	22.9	25.3	20.8	17.8	17.2	7.5	36.6
Ce	63.7	68.7	55.1	37.5	36.5	19.4	75.2
Pr	9.6	10.4	8.2	4.9	4.8	2.9	9.1
Nd	44.6	45.4	37.2	21.2	21.2	14.3	33.8
Sm	10.4	10.2	8.9	5.7	5.6	4.4	6.6
Eu	2.8	3.2	2.6	1.6	1.8	1.5	1.7
Gd	8.5	8.9	7.5	5.1	5.6	5.2	6.1
Tb	1.3	1.2	1.1	0.8	0.9	0.9	0.9
Dy	6.2	6.1	5.5	4.7	5.4	5.4	4.8
Ho	1.1	1.2	1.0	0.9	1.1	1.1	1.0
Er	3.1	3.1	2.7	2.5	2.8	2.8	2.7
Tm	0.4	0.4	0.4	0.3	0.4	0.4	0.4
Yb	2.7	2.6	2.3	2.0	2.4	2.4	2.5
Lu	0.4	0.4	0.3	0.3	0.4	0.4	0.4
Y	29.0	35.1	26.0	24.1	26.2	28.3	29.7
Rb	647.0	620.8	429.0	287.0	333.0	5.6	190.1
Ba	1311.0	931.8	870.0	2209.0	862.0	563.0	1079.4
Th	3.5	3.0	3.0	2.7	2.5	0.9	8.1
U	0.9	0.8	0.7	0.5	0.5	0.3	2.2
Ta	0.4	0.5	0.3	1.2	1.2	0.5	0.8
Nb	5.5	7.3	4.6	17.1	19.4	7.0	13.6
Sr	468.0	638.6	527.0	314.0	666.0	986.0	665.0
Zr	182.0	200.8	160.0	138.0	142.0	107.0	194.6
Hf	5.0	4.2	4.3	3.9	4.1	3.3	4.3
Ni	39.2	77.5	72.6	80.4	119.0	74.0	21.6
Cr	113.0	309.6	249.0	165.0	272.0	77.5	43.8
$Mg^{\#}$	0.59	0.49	0.63	0.46	0.48	0.43	0.49
$(La/Sm)_N$	1.42	1.60	1.51	2.02	1.99	1.11	3.58
Eu/Eu^*	0.89	1.01	0.95	0.90	0.94	0.96	0.83
Ce/Ce^*	1.05	1.04	1.04	0.97	0.97	1.03	0.98

Abbreviations: WX, Weixi ore block; M, Main ore block; WD, Weidong ore block. $Eu/Eu^* = Eu_N/[(Sm + Gd)_N/2]$; $Ce/Ce^* = Ce_N/[(La + Pr)_N/2]$. N-chondrite-normalized ratio.

Dynamics, CAGS. Helium was used as the carrier gas during the analysis and international standard zircon samples GJ–1 were used as reference. Detailed analytical procedures were similar to those described by Wu et al. (2006).

4. Results

4.1. Zircon U–Pb geochronology

Sample 9901G (basalt from the Weixi ore block): Zircons separated from sample 9901G are mostly prismatic and euhedral in morphology ranging from 150 × 40 μm to more equant 40 × 40 μm grains, and transparent and light brown in color (Fig. 5). The CL images show that only few zircons within the sample are characterized by an inherited core and a rim with oscillatory zoning (Fig. 5; grain 9901G-5), others have commonly concentric oscillatory zoning with low to variable luminescence (Fig. 5), an indicative of magmatic origins. Fourteen single grains of zircon with different textures were analyzed, giving a wide range in uranium (65–875 ppm) and thorium (56–260 ppm) contents, as well as Th/U ratios ranging from 0.07 to 1.07 (mostly 0.38–0.71) (Table 2). A subset of three grains with core-rim structures yields variably Mesoproterozoic to Neoproterozoic dates (1463.0–920.6 Ma), probably owing to core-rim overlap. They roughly represent the crystallization ages of inherited or captured zircons entrained by the basalt, similar to the age of wall rocks (i.e., the Langyashan Formation) in the Weibao district. The remaining data define a linear array on the concordia diagram (Fig. 6) and are anchored by a cluster of concordant analyses, yielding a weighted mean $^{206}Pb/^{238}U$ data of 392.0 ± 5.0 Ma (Fig. 6). This age represents the timing of eruption of volcanic rocks.

Sample WD55 (basaltic andesite from the Weidong ore block): Zircons of sample WD55 are generally euhedral and prismatic in morphology, and transparent and pale yellow in color with 40–160 μm in length and 30–60 μm in width (Fig. 5). Zircon analysis results of this sample are very similar to those of sample 9901G, and the interpretation is therefore identical. The well-developed tetragonal dipyramids and oscillatory zoning in zircon crystals of sample WD55, manifested by the CL images, suggest an igneous origin. This is further confirmed by relatively high Th/U ratios of these zircons (0.37–1.28). Minor zircons, however, manifest a core-rim structure (Fig. 5; grain WD55-6), similar to that in sample 9901G. Zircon grains of sample WD55 have a highly

wide range in uranium (111–3830 ppm) and thorium (49–1687 ppm) concentrations (Table 2). Among fifteen zircon grains analyzed, grains 3 and 6 yield disconcordant ages (966.6–1092 Ma) that can be interpreted to be ages of inherited or captured zircons entrained by the volcanic rocks. The remaining 13 zircon grains form a cluster on the concordia plot with a weighted mean $^{206}Pb/^{238}U$ age of 393.0 ± 5.5 Ma (Fig. 6). This is the best estimate of the age of volcanic eruption.

Overall, our SHRIMP U–Pb zircon dating results indicate that the lavas within the Weibao deposit are synchronous and erupted at around 393 Ma.

4.2. Whole–rock geochemistry

Major and trace element analyses are presented in Table 3.

The relatively high loss on ignition (LOI; 1–5 wt.%) manifests the existence of weathering and/or calcite inclusions within the lavas. These volcanic rocks have a wide range of SiO_2, MgO, Fe_2O_3 and CaO compositions, with SiO_2 = 46.45–55.75 wt.%, MgO = 3.71–7.52 wt.%, Fe_2O_3 = 7.78–13.96 wt.% and CaO = 4.66–9.88 wt.%. In contrast, the concentrations of Al_2O_3 (13.32–15.45 wt.%), TiO_2 (0.96–2.15 wt.%), P_2O_5 (0.16–0.47 wt.%) and MnO (0.12–0.21 wt.%) are relatively consistent. Besides, apart from sample WD-104 showing low alkali contents (K_2O = 0.2 wt.%, K_2O + Na_2O = 2.97 wt.%), the remaining samples are high in total alkalis (K_2O = 2.70–6.18 wt.%, K_2O + Na_2O = 6.19–7.18 wt.%). We have classified the lavas using the total alkalis (K_2O + Na_2O) vs SiO_2 (TAS) classification diagram (Fig. 7). All the samples, with the exception of sample WD–104 (plotting in sub-alkaline basalt field), fall into the alkaline field and classify as tephrite basanite, trachybasalt and basaltic trachy-andesite. However, we suspect that the alkaline character of these volcanic rocks is not primary and might have been introduced by potassic alteration, as described in Section 3.1. The absence of common alkaline minerals, e.g., feldspathoids (nepheline, leucite and sodalite), also demonstrates that this alkaline character of the Weibao volcanic rocks is not primary. In Harker variation diagrams (Fig. 8), MgO, MnO and CaO display constant decreases with increasing SiO_2, whereas other major elements do not show unified variation trends.

In chondrite-normalized rare earth elements (REE) diagrams (Fig. 9a–c), Eu anomalies are not present within all samples, indicating that they did not experience fractional crystallization of feldspar. Besides, most of the basalt samples are enriched in light rare earth element (LREE) [$(La/Sm)_N$ = 1.4–3.6; generally 1.4–2.0; Table 3], thus manifesting LREE-enriched patterns (Fig. 9a–c), whereas sample WD-104 displays a relatively flat pattern in chondrite-normalized diagram [$(La/Sm)_N$ = 1.1] (Fig. 9c). Noticeably, the samples with high LREE generally display evident enrichment in Rb, Ba and K contents and depletion in Th, U, especially Nb and Ta contents relative to the adjacent large ion lithophile elements (LILE) and high field strength elements (HFSE) in primitive mantle-normalized patterns (e.g., Fig. 6d). Specially, with the exception of Ba and Sr, sample WD–104 also manifests a relatively flat pattern in Fig. 9f.

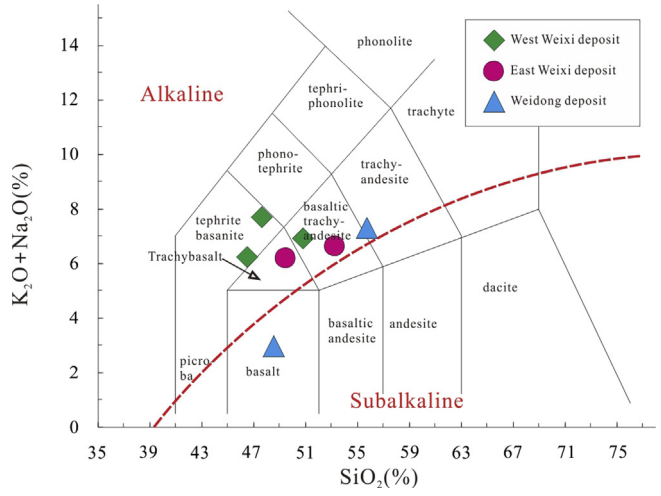

Fig. 7. Total alkalis (K_2O + Na_2O) vs SiO_2 (TAS) classification diagram of volcanic rocks from the Weibao deposit (boundaries after Le Bas et al., 1986). We suggest that the alkaline feature displayed by the majority of the volcanic rocks from the Weibao deposit is mainly caused by alteration. See Sections 3.1 and 4.2 for details.

4.3. Zircon Hf isotopes

Zircon Hf isotope analyses for the volcanic rocks of the Weibao deposit are given in Table 4.

Sample 9901G: Eleven spot analyses were obtained for sample 9901G from the Weixi ore block, with $^{176}Hf/^{177}Hf$ ratios exhibiting a relatively wide isotopic range from 0.28247 to 0.28276. Spots 2 and 14 give negative εHf(T) values of −2.6 and −1.0 respectively, whereas the remaining 9 spots show positive values ranging from +0.9 and +7.3 (mostly +2.9–+6.0). Therefore, in Fig. 10 the εHf(T) values of sample 9901G display a bimodal distribution.

Sample WD–55: 13 spot analyses were obtained for sample WD–55 from the Weidong ore block. Similar to sample 9901G, the majority of zircons yield $^{176}Hf/^{177}Hf$ ratios between 0.28261 and 0.28276, corresponding to εHf(T) values between +1.8 and +7.5 (mostly +3.4–+6.9). This is noticeably deviated with the other two spots displaying low $^{176}Hf/^{177}Hf$ ratios (0.28245–0.28251) and negative εHf(T) values (−2.0 to −1.2). Likewise, a nearly bimodal distribution pattern is shown for the εHf(T) values of sample WD55 (Fig. 10).

5. Discussion

5.1. Screening for alteration

In order to identify primary geochemical signatures for evaluating petrogenesis and geodynamic setting, it is essential to eliminate the effects resulted from alteration and metamorphism (e.g., Manikyamba et al., 2009). To achieve this objective, careful sample collection and selection based on field documentation and mineralogical-geochemical assessment of alteration features is pivotal. For the volcanic rocks from the Weibao deposit, least altered samples for geochemical analysis were selected based on petrographical preservation of primary igneous textures and absence of amygdaloidal textures, therefore ensuring the accuracy and representativeness of the geological survey. Selecting suitable geochemical diagrams is another important aspect, as suggested by Pearce (1996). Post-eruption element mobility might result in highly variable alkali contents of the Weibao volcanic rocks, thus reducing the credibility of TAS (Fig. 7) and SiO_2 vs. K_2O diagrams (not shown). In contrast, it has been demonstrated that REE, HFSE, V, Al and Sc remain unaffected in rocks which have suffered alteration and greenschist facies metamorphism (e.g., Manikyamba et al., 2009; Pearce and Norry, 1979). Accordingly, the magmatic affinities of igneous rocks can be determined by the values and trends of these major and trace elements (e.g., Pearce, 1982; Squire et al., 2006 and references therein). In this study, the majority of diagrams are therefore based on the immobile elements rather than the usual major elements, such as Mg, Na, K and Si, which are alteration-dependent (Pearce, 1996). Nevertheless, Pearce (1982) argued that immobile element (e.g., LREE) might also become mobile by increased temperature and the formation of chloride, and other, complexes. For the Weibao volcanic rocks, this

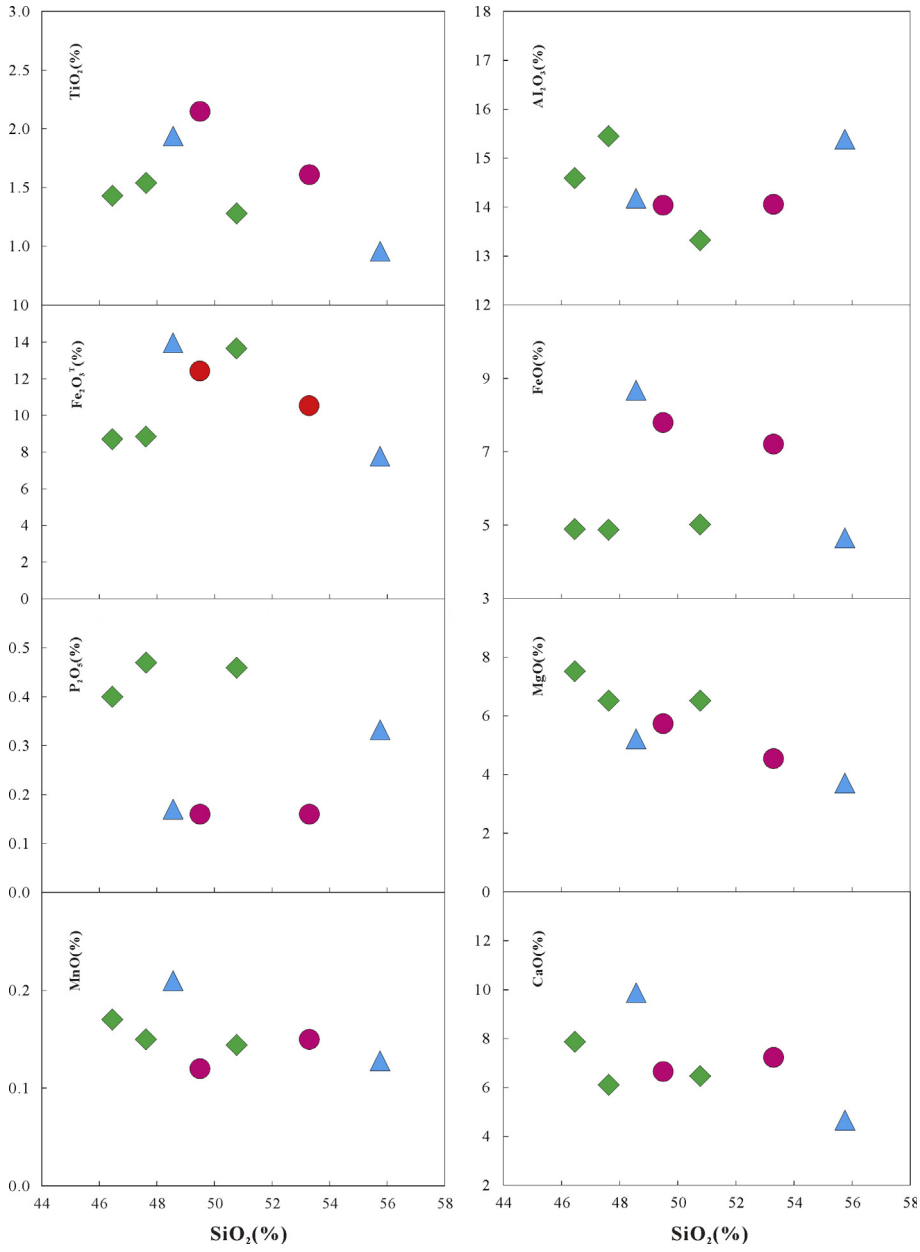

Fig. 8. Harker diagrams showing the variations in major element behaviors with increasing SiO_2. The symbols are as in Fig. 7.

scenario can be precluded in terms of the LREE mobility evaluated by Ce/Ce* ratios. Generally, mafic volcanic rocks having Ce/Ce* ratios between 0.9 and 1.1 manifest limited LREE mobility whereas those with Ce/Ce* < 0.9 and >1.1 are characterized by LREE mobility (Polat and Kerrich, 2002; Manikyamba et al., 2009). Consequently, the indistinctive Ce anomalies (Ce/Ce* = 0.97–1.05) of the volcanic rocks from the Weibao deposit, as well as the highly coherent REE patterns (Fig. 9a–c) and relatively consistent multi-element patterns (Fig. 9d–f), firmly endorse limited mobility of those elements.

5.2. Implication of SHRIMP zircon U–Pb ages

The SHRIMP zircon U–Pb ages that we report in this study can be subdivided into two groups. One group displays old ages (1.4–0.9 Ga) that are consistent well with the age of the host rock in the Weibao deposit. Therefore, these ages could be interpreted to represent ages of inherited or captured zircons entrained by the volcanic rocks. The other age group of ~393 Ma is dominant and much younger, which could represent the age of volcanic eruption. It might be suspected that this young age have resulted from retrograde overprint of alteration and greenschist facies metamorphism. We, however, consider this to be unlikely for the following reasons: (1) most analyzed zircon grains develop concentric oscillatory zoning as well as high Th/U ratios (mostly 0.38–0.71), and thus can be noticeably distinguished from metamorphic zircons that usually have rounded shape and low Th/U ratios (e.g., Vavra et al., 1996); (2) the upper limit of metamorphism temperatures of greenschist facies is 550–525 °C (Winkler, 1957), whereas the closure temperature of uranium and lead isotopic system in zircon is ca. 850 °C and/or even higher (Lee et al., 1997; Cherniak and Watson, 2001; Coleman et al., 2004; Hourigan et al., 2004; Flowers et al., 2005). Thus, subsequent alteration and greenschist facies were obviously not strong enough to cause resetting of the uranium and lead isotopic system in zircon. Consequently, we confirm that the basaltic rocks in the Weibao

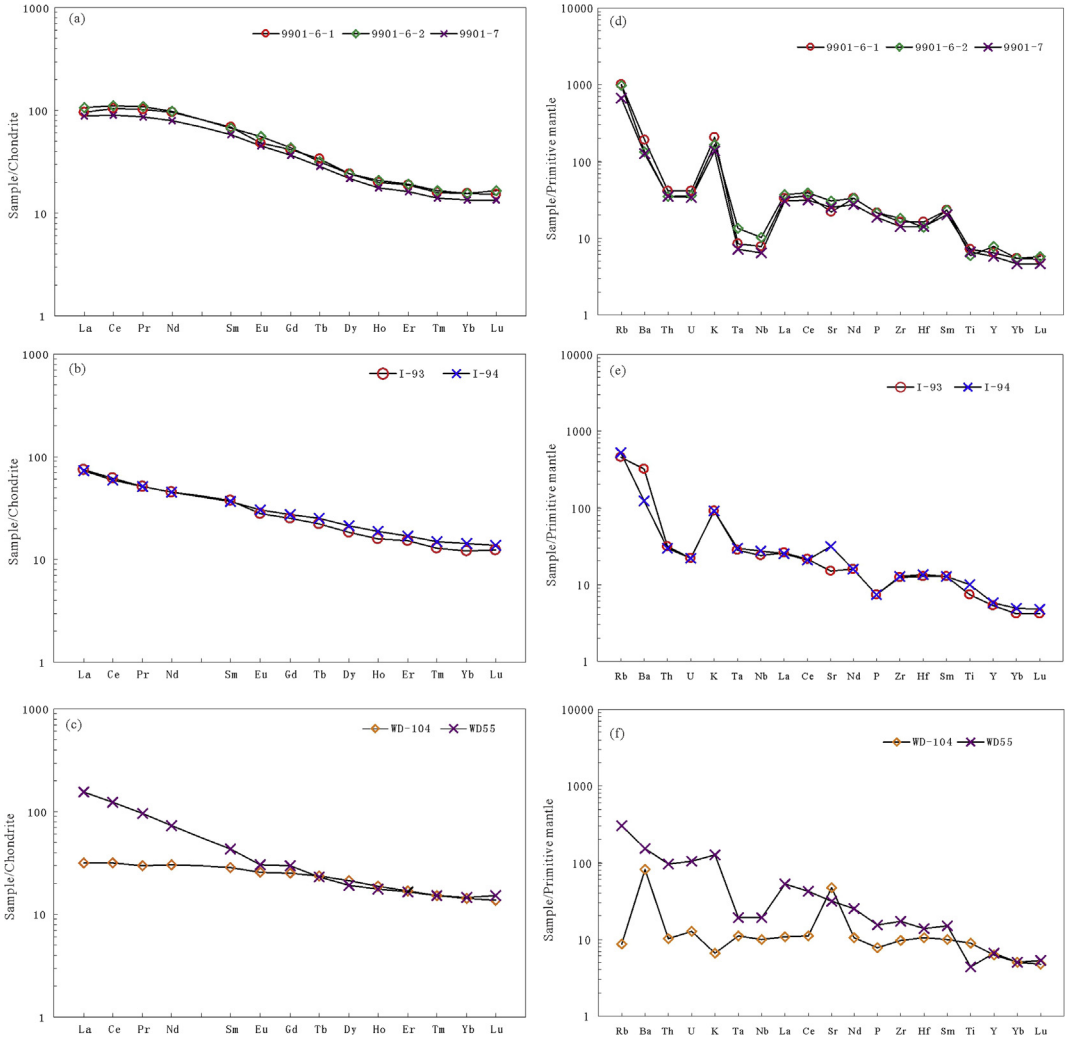

Fig. 9. Chondrite-normalized REE (a–c) and primitive mantle-normalized trace element diagrams (d–f) for the volcanic rocks from the Weibao deposit. The chondrite and PM values are from Sun and McDonough (1989).

deposit erupted in Middle Devonian. Combined with our unpublished dating data with regard to porphyritic granites (~408 Ma) in the Weibao deposit, it can be inferred that igneous events were active in Early to Middle Devonian in the Weibao district.

Actually, the Early–Middle Devonian igneous activity did not only occur in the Weibao area. Large numbers of geochronological data have revealed that igneous activities coeval with basaltic eruption in the Weibao deposit are widespread along the entire EKOB. Wang et al. (2013) reported a syenogranite U–Pb age of 391.1 ± 1.4 Ma in the Xiarihamu district; Gao et al. (2014b) reported monzogranite and granodiorite U–Pb ages of 393 ± 2 Ma and 386 ± 1 Ma respectively in Yemaquan district; Hao et al. (2015) showed that granite porphyry in the Qunli district formed in 391.3 ± 3.2 Ma; newly discovered mafic dyke swarms in the eastern section of the EKOB were also demonstrated to form in Middle Devonian (~393 Ma; Xiong et al., 2014). Besides, mafic intrusions, such as gabbro in Kayakedengtage complex, are also confirmed to form simultaneously (403.3 ± 7.2 Ma; Chen et al., 2006). Apart from these intrusions, the Devonian volcanic eruption was further manifested by the occurrence of rhyolite (432–400 Ma; Lu et al., 2010) and dacite (406.1 ± 2.9 Ma; Zhang et al., 2010) in the Maoniushan Formation. All these data, together with ages obtained by this study, indicate strong interactions between crust and mantle during Early–Middle Devonian in the EKOB.

5.3. Role of fractional crystallization in petrogenesis

Although the effects of fractional crystallization can be very difficult to distinguish from those of partial melting, the use of compatible–incompatible elements plots may still be useful. The abundances of compatible elements (e.g., Ni and Cr) and incompatible elements (e.g., Th, La and Nd) in the magmas would be expected to decrease and increase respectively when ferromagnesian minerals such as olivine, clinopyroxene and amphibole are fractionated from the magmas (e.g., Aldanmaz et al., 2000). The plots in Fig. 11 display that increases in compatible and decreases in incompatible element concentrations are accompanied by decreasing of SiO_2 contents. This just matches well with the evolution trend expected during fractional crystallization.

The behavior of fractionation can also be constrained by Rb–Y diagram (Fig. 12). Different from rubidium, yttrium generally strays broadly constant at mafic–intermediate compositions, which can be illustrated by amphibole fractionation (Lambert et al., 1974; Pearce et al., 1990). Therefore, the nearly constant Y contents with increasing of Rb contents in the Weibao volcanic rocks confirm the significant fractionation of amphibole in the origin of these rocks. This is also supported by the negative correlations of MgO, MnO and CaO with increasing SiO_2 which result from amphibole fractionation. Amphibole can be a liquidus phase

Table 4
Zircon *in situ* Hf isotopic data of the lavas from the Weibao deposit.

Sample	$^{176}Yb/^{177}Hf$	$^{176}Lu/^{177}Hf$	$^{176}Hf/^{177}Hf$	2σ	$^{176}Hf/^{177}Hf_i$	εHf(0)	εHf(T)	2σ	$f_{Lu/Hf}$
9901G									
9901G-01	0.042480	0.001358	0.282574	0.000019	0.282564	−7.4	0.9	0.68	−0.96
9901G-02	0.015339	0.000450	0.282467	0.000016	0.282464	−11.2	−2.6	0.57	−0.99
9901G-03	0.077534	0.002264	0.282636	0.000021	0.282619	−5.3	2.9	0.76	−0.93
9901G-04	0.037566	0.001166	0.282658	0.000021	0.282650	−4.5	4.0	0.75	−0.97
9901G-07	0.061015	0.001848	0.282649	0.000022	0.282635	−4.8	3.4	0.76	−0.95
9901G-09	0.092596	0.002919	0.282728	0.000018	0.282707	−2.0	6.0	0.62	−0.91
9901G-10	0.048077	0.001544	0.282755	0.000018	0.282743	−1.1	7.3	0.63	−0.95
9901G-11	0.041592	0.001373	0.282666	0.000016	0.282656	−4.2	4.2	0.58	−0.96
9901G-12	0.066151	0.002003	0.282711	0.000019	0.282696	−2.6	5.6	0.68	−0.94
9901G-13	0.045608	0.001491	0.282659	0.000022	0.282648	−4.4	3.9	0.78	−0.96
9901G-14	0.048814	0.001644	0.282521	0.000022	0.282509	−9.3	−1.0	0.77	−0.95
WD55									
WD55-01	0.053412	0.001667	0.282762	0.000020	0.282750	−0.8	7.5	0.7	−0.95
WD55-02	0.070224	0.002234	0.282728	0.000017	0.282711	−2.0	6.2	0.6	−0.93
WD55-04	0.126605	0.004191	0.282619	0.000022	0.282588	−5.9	1.8	0.8	−0.88
WD55-05	0.043323	0.001404	0.282725	0.000019	0.282715	−2.1	6.3	0.7	−0.96
WD55-07	0.047884	0.001507	0.282674	0.000017	0.282663	−3.9	4.4	0.6	−0.96
WD55-08	0.045165	0.001432	0.282743	0.000020	0.282732	−1.5	6.9	0.7	−0.96
WD55-09	0.116084	0.003645	0.282736	0.000021	0.282709	−1.7	6.1	0.7	−0.89
WD55-10	0.045211	0.001440	0.282644	0.000016	0.282633	−5.0	3.4	0.6	−0.96
WD55-11	0.032635	0.000997	0.282510	0.000019	0.282502	−9.7	−1.2	0.7	−0.97
WD55-12	0.064204	0.002021	0.282653	0.000024	0.282639	−4.7	3.6	0.85	−0.94
WD55-13	0.068391	0.002170	0.282743	0.000020	0.282727	−1.5	6.7	0.7	−0.94
WD55-14	0.018822	0.000630	0.282707	0.000019	0.282703	−2.7	5.8	0.7	−0.98
WD55-15	0.039088	0.001088	0.282489	0.000023	0.282481	−10.5	−2.0	0.8	−0.97

T = 393 Ma, roughly representing the crystallization age of the basalts within the Weibao district. $\lambda = 1.867 \times 10^{-11}$ $year^{-1}$, decay constant of ^{176}Lu (Söderlund et al., 2004). The $^{176}Hf/^{177}Hf$ and $^{176}Lu/^{177}Hf$ ratios of chondrite and depleted mantle at the present are 0.282785 and 0.0336, and 0.28325 and 0.0384, respectively (Bouvier et al., 2008 and Griffin et al., 2000).

in basaltic to basaltic–andesite magmas under near water-saturated conditions (>10 wt.% H_2O at 15 kb) at depths of around 25–80 km (8–25 kb) (Pearce et al., 1990). With the uplifting of these magmas, crystallization should initially be amphibole-dominated with subordinate minerals, such as pyroxene and magnetite. This hydrous, amphibole-bearing crystallization history is further illustrated by the REE patterns showing no increase or a decrease of the MREE and HREE, analogous to that found within the volcanic rocks from Eastern Anatolia (Pearce et al., 1990).

Overall, the major and trace element behaviors can thus be seen to highlight a hornblende-dominated fractionation during eruption of volcanic rocks. However, the majority of major elements plot scattered in Harker diagrams (Fig. 8), indicating that the genesis of these basaltic volcanic rocks cannot be fully explained by the single mechanism of fractional crystallization. Other mechanisms, such as partial melting, must also play an important role in the generation of these basaltic magmas.

5.4. The sources of early paleozoic–middle Devonian magmatism in the EKOB

5.4.1. Crustal contamination?

The role of crustal contamination must be considered since basaltic magmas are eventually emplaced in a continental setting. Generally, crustal contamination would result in increases of SiO_2, and decreases of MgO and Mg# in melts. Volcanic rocks from the Weibao deposit display low SiO_2 (46.45–55.75 wt.%), and high MgO (3.71–7.52 wt.%) and Mg# (0.43–0.63), therefore ruling out significant crustal contamination. Additionally, crustal contamination can result in Th/Yb ratios correlating with silica content (Aldanmaz et al., 2000), whereas the Th/Yb ratios of the Weibao volcanic rocks are extremely scattered with the increasing silica content in Fig. 13 (shown as inset diagram). Moreover, since Precambrian gneiss in the EKOB is characterized by extremely enriched initial εHf(T) values (−12 to −15; Chen et al., 2007), incorporation of even a small amounts of this old continental components in the melts would remarkably change their isotopic compositions. However, zircon initial εHf(T) values of volcanic rocks from the Weibao deposit are much higher, ranging from −2.6 to +7.5 (mostly +3.4 to +7.5), therefore further indicating that the geochemical composition of the Weibao volcanic rocks cannot be shifted enough by crustal contamination to mask the character of their mantle source.

In conclusion, we argue that contributions from crustal contamination are negligible for the Weibao volcanic rocks and their compositions can therefore be used to study their mantle source.

5.4.2. The mantle source of volcanic rocks in the Weibao deposit

Magmatic rocks derived from depleted mantle should be characterized by positive εNd(T) values and extremely high εHf (T) values (normally >+10) (Fig. 14). However, zircon initial εHf (T) values of volcanic rocks from the Weibao deposit are relatively low, ranging from −2.6 to +7.5 (mostly +3.4 to +7.5). Normal convecting asthenospheric mantle with a depleted mantle-like isotopic composition therefore cannot account for those low εHf(T) ratios, as well as the observed features of trace and rare earth elements (e.g., strong depletion of HFSE). Rather, this feature can only be reconciled by mixing between the depleted mantle and crustal components in their sources, although the overwhelmingly positive εHf(T) values of zircons indicate that they should be predominantly derived from depleted mantle (and hence asthenospheric mantle).

Previous works have illustrated that subducted components (fluids derived from slab dehydration and/or melts derived from subducted sediments) can result in the "crustal" signature in the magma source (e.g., Gasparon and Varne, 1998). Besides, rocks originating from the mantle enriched by subducted components display selective enrichment in LILE (such as Sr, K, Rb, Ba, Th and LREE) relative to HFSE (e.g., Pearce et al., 1990; Weaver, 1991; Cervantes and Wallace, 2003; Mazzeo et al., 2014). Moreover, a mantle source will show a significant increase in Th/Yb ratios but indistinctive shift on Ta/Yb ratios if they are enriched by

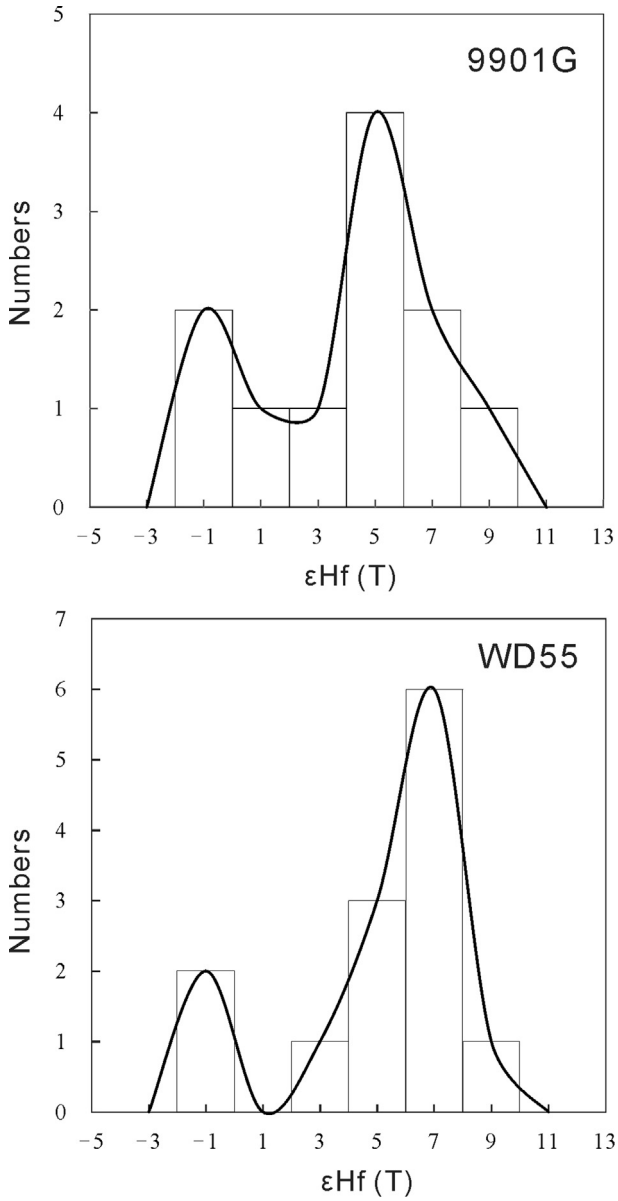

Fig. 10. Histogram of εHf(T) values for zircons from volcanic rocks in the Weibao deposit.

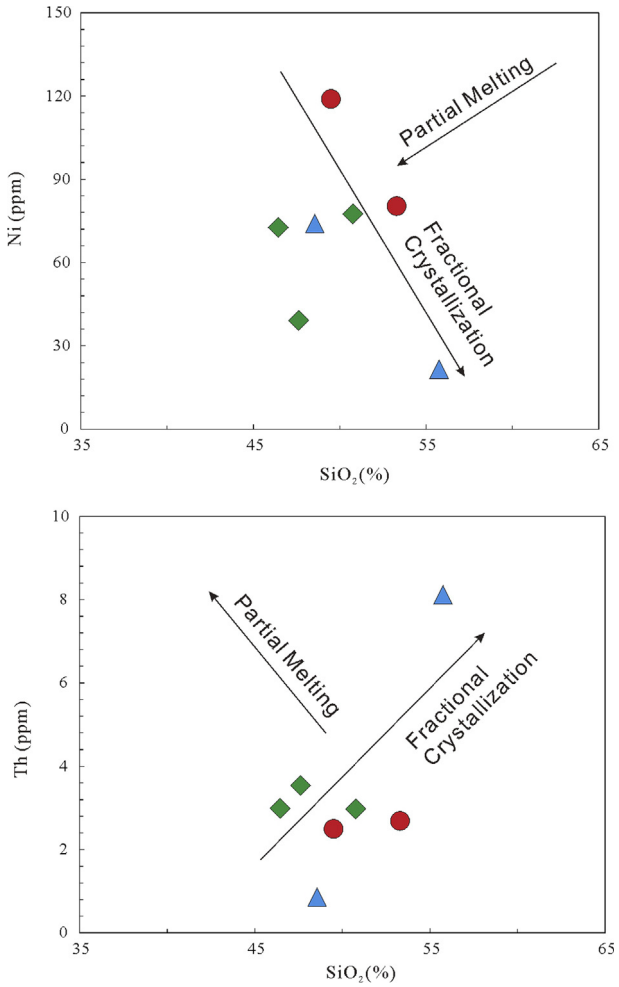

Fig. 11. (a) Ni (compatible element); and (b) Th (highly incompatible element) plots against SiO_2 showing possible fractional crystallization and partial melting trends for the volcanic rocks from the Weibao deposit. The symbols are as in Fig. 7.

slab-induced fluids (Pearce et al., 1990; Pearce and Peate, 1995; Gorton and Schandl, 2000). The Weibao volcanic rocks are selectively enriched in LILE relative to HREE (Fig. 9). On Ta/Yb against Th/Yb diagram (Fig. 13), all the samples within the Weibao deposit display high Th/Yb ratios relative to mantle array, forming a roughly vertical trend. These features match well with those of volcanic rocks generated by arc volcanism. Numerous studies have suggested that igneous rocks with volcanic arc-like signatures do not necessarily imply a subduction setting (e.g., Pearce et al., 1990; Notsu et al., 1995; Peccerillo, 1998; Aldanmaz et al., 2000; Xia, 2014; Wang et al., 2016); rather, they might be associated with magma sources enriched by pre-collision subduction events (Pearce et al., 1990; Notsu et al., 1995; Peccerillo, 1998; Aldanmaz et al., 2000). It is very likely that the Weibao volcanic rocks were produced in such a similar regime considering that they are virtually generated in a post-collisional environment (see Section 5.5 for more details). If this interpretation is correct, the enriched isotopic feature [e.g., low εHf(T) values] of the Weibao volcanic rocks might be most probably generated by the sediments and/or fluids introduced by the subducted slab, just like that found in the Variscan French Massif Central where the post-collisional mafic magmatism was believed to be derived from a hybrid source comprising of depleted mantle and subducted components (Couzinié et al., 2016).

To understand the whole evolution process of the Weibao region, the remaining task is to quantify the relative contribution of two dominant end-members (and hence asthenospheric mantle and subducted components). Currently, it is not yet possible, however, to model this because of the lack of systematic isotopic data (e.g., Sr–Nd–Pb).

5.4.3. The sources of Early paleozoic–middle Devonian magmatism in the EKOB

In Fig. 14, initial εHf(T) values are shown for the Early Paleozoic–Middle Devonian igneous rocks in the EKOB. Despite of the discrepancies of rock types, it is displayed that identical to the ~393 Ma volcanic rocks in this study, Early Paleozoic–Middle Devonian magmatic rocks in the EKOB are also characterized by moderate εHf(T) ratios (mostly −3 to +10) which therefore might indicate a similar genesis among them. This is further demonstrated by the consistent Sr–Nd isotopes for the Early Paleozoic–Middle Devonian magmatic rocks in the EKOB that are all characterized by slightly enriched initial $^{87}Sr/^{86}Sr$ (0.7054 to

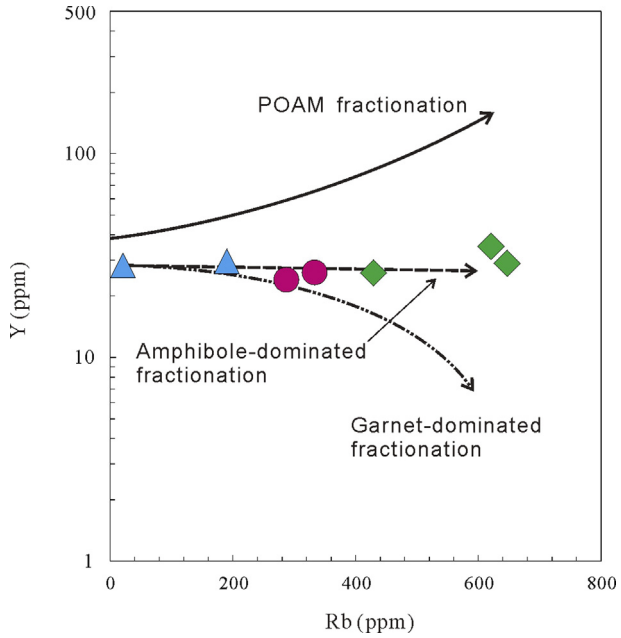

Fig. 12. Rb–Y diagram highlighting the fractionation process. Three distinct trends commonly can be recognized, as illustrated by Pearce et al. (1990): the trend of increasing Y and Rb (the bold solid line) which could be interpreted as dominated by POAM (plagioclase, olivine, pyroxene, magnetite) fractionation; a trend of nearly constant Y (the dashed line) best explained in terms of amphibole-dominated fractionation; and a declining trend (the dot dash line) best explained in terms of fractionation involving garnet. Note that the samples from the Weibao deposit match well with the amphibole-dominated fractionation trend. The symbols are as in Fig. 7.

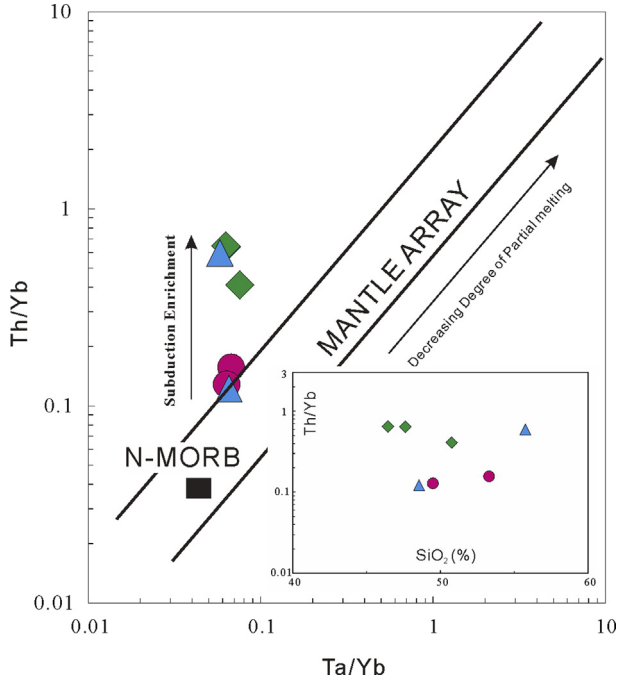

Fig. 13. Ta/Yb vs Th/Yb diagram for the volcanic rocks from the Weibao deposit (modified after Pearce et al., 1990; Aldanmaz et al., 2000; and references therein). The diagonal trend (i.e., mantle array) constrained by constant Th/Ta ratios represents basaltic magmas derived from the mantle asthenosphere (and hence depleted mantle), plume asthenosphere or mantle lithosphere modified by melts from asthenosphere. Note that the samples from the Weibao deposit exhibit a consistent displacement from the mantle array indicating subduction-related metasomatism. The inset diagram shows the variations of Th/Yb with changing silica contents of the rocks. See Section 5.4.2 for further discussions. The symbols are as in Fig. 7.

0.7240) and εNd(T) values (−5.3 to +3) compared to depleted mantle (Liu et al., 2013; Zhang et al., 2014; Xiong et al., 2015). Combined with major and trace elements of the Xiadawu appinitic pluton, Xiong et al. (2015) suggested that those enriched feature indicated a depleted mantle source which was metasomatised by subducted sediment-derived felsic melts, which is just like that for the Weibao volcanic rocks. A similar interpretation emphasizing hybridization in the source was also proposed by Hao et al. (2015) for the Devonian post-collisional granitoids in the EKOB.

Collectively, we argue that Early Paleozoic–Middle Devonian magmatism in the EKOB has similar magmas sources that are characterized by mixing of depleted mantle and crustal components (especially subducted components) with variable ratios. This feature also manifests strong interaction between mantle and crust during Early Paleozoic–Middle Devonian magmatic rocks in the EKOB, which might play an important role in the crustal evolution in the EKOB (e.g., Couzinié et al., 2016).

5.5. Tectonic setting

The trace element diagrams, especially those constrained by HFSE such as Ta, Th, Nb, Zr, can successfully identify tectonic environments of basaltic rocks. In this study, Cr–Y, Hf/3–Th–Nb/16, and Zr/Y–Zr diagrams (Fig. 15) are employed to examine the tectonic setting of the Weibao volcanic rocks. The samples plot mainly within the transitional field of VAB and WPB in Cr–Y and Hf/3–Th–Nb/16 diagrams (Fig. 15a, b). In Zr/Y–Zr diagram (Fig. 15c), with the exception of sample WD–104, all the others plot into WPB field. Pearce (1996) suggested that volcanic rocks with features (plotting in both the VAB and WPB fields) were most likely to have erupted in a post-collisional setting. For the Middle Devonian Weibao volcanic lavas, a post-collisional setting rather than a subduction environment is further demonstrated by the following evidence. (1) Although the exact closure time of the Proto-Tethys Ocean in the EKOB is controversial, the occurrence of *syn*-collision granitoids with ages of 430.8 Ma to 428.5 Ma (Cao et al., 2011; Wu et al., 2012) and deposition of molasses sediments of the Maoniushan Formation (ca. 423–400 Ma; Lu et al., 2010; Zhang et al., 2010) suggest that subduction had ceased before Devonian; therefore, the Middle Devonian Weibao volcanic rocks could not form in a subduction setting. (2) Early to Middle Devonian granitoids in the EKOB are represented by Yemaquan granodiorite (403.7 ± 2.9 Ma), Qunli granite porphyry (391.3 ± 3.2 Ma), Kayakedengtage granodiorite (380.52 ± 0.92 Ma) and Yuejinshan granodiorite (407 ± 3 Ma), all of which were confirmed to be post-collisional granitoids (Liu et al., 2012; Hao et al., 2015). (3) Moreover, Early Devonian mafic igneous activities in the Yuejinshan area were also demonstrated to be related to the extension in a post-collisional setting (Liu et al., 2012). Therefore, a post-collisional setting is reasonable to explain the genesis of the Middle Devonian Weibao basaltic lavas.

Recently, two tectonic models with regard to the evolution of the Qimantagh area during Early Paleozoic to Devonian were proposed by Hao et al. (2015) and Meng et al. (2015), respectively. The former successfully illustrated most tectono-magmatic events during this period, whereas the history with regard to the post-collisional stage of the Qimantagh area was not mentioned in this model. The other model proposed by Hao et al. (2015) emphasised the evolution from syn- to post-collisional stages during Early Paleozoic within the Qimantagh area, but the evolution process before the collision between the NEKT and Qaidam terrain (QT) was not well displayed. Therefore, it is necessary to reconstruct an Early Paleozoic to Devonian tectonic model in order to better understand the overall geodynamic evolution from subduction to post-collision in this region.

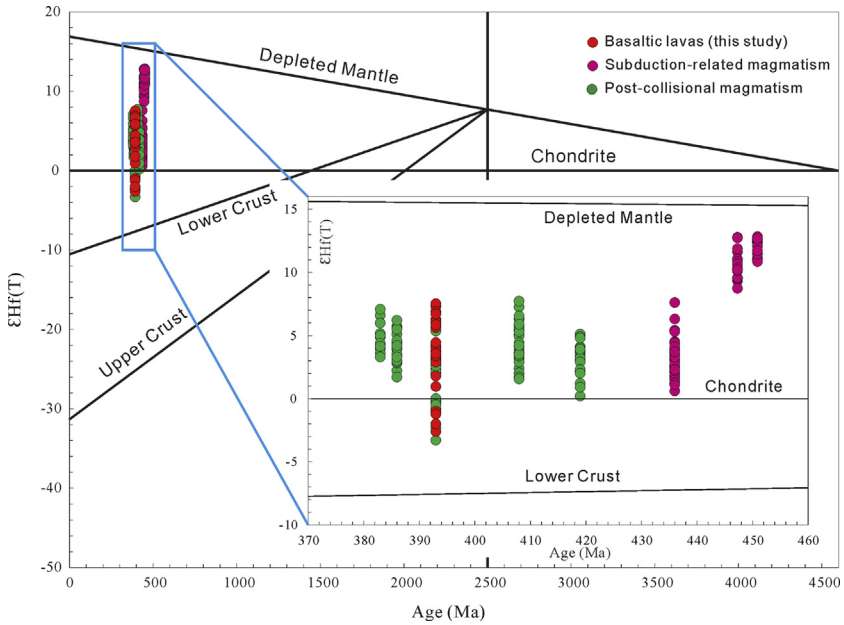

Fig. 14. Compilation of available in-situ Hf isotope data for zircons from the EKOB as a function of their intrusion age. Data sources: the 393 Ma monzonitic granite and the 386 Ma granodiorite in the Yemanquan district (Gao et al., 2014b); the ~393 Ma mafic dykes in the east of the EKOB (Xiong et al., 2014); the ~447 Ma and 450.9 Ma appinites in the Xiadawu pluton (Xiong et al., 2015); the 436 Ma granodiorite in the Buqingshan tectonic mélange belt (Li et al., 2015); the 383 Ma diabase, 408 Ma porphyritic granite (unpublished data) and ~393 Ma basaltic lavas (this study) in the Weibao district. Subducted-related and post-collisional magmatism is subdivided according to Section 5.5.

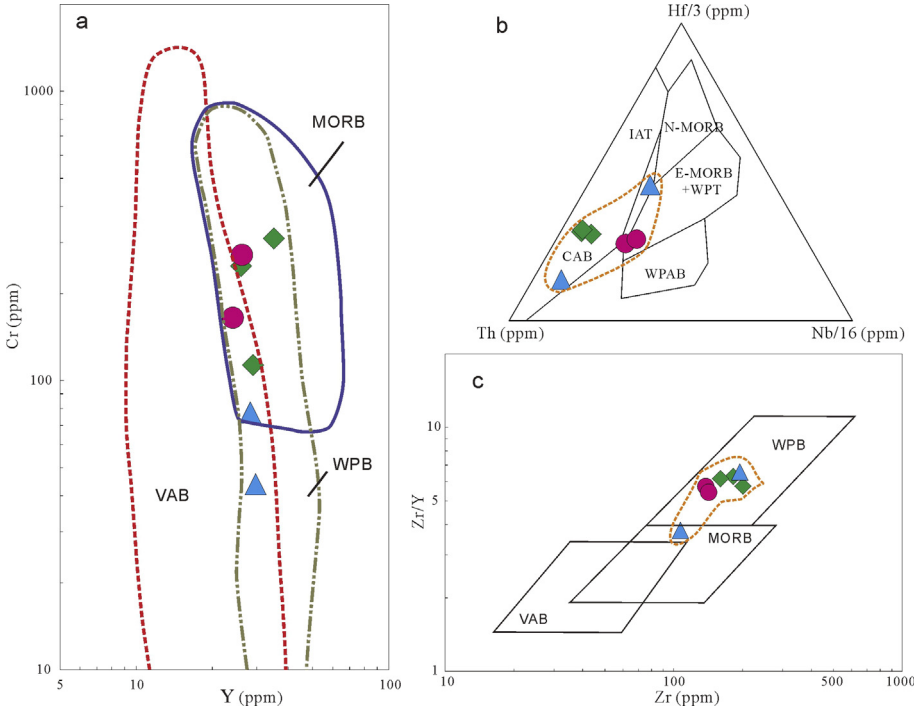

Fig. 15. Tectonic discrimination diagrams for the volcanic rocks within the Weibao deposit. (a) Y–Cr diagram (Pearce, 1982). (b) Hf/3–Th–Nb/16 diagram (Wood, 1980). (3) Zr–Zr/Y diagram (Pearce and Norry, 1979). Abbreviations: VAB–volcanic arc basalts; MORB–mid-ocean ridge basalts; N-MORB–normal mid-ocean ridge basalts; E-MORB–enriched mid-ocean ridge basalts; WPB–within-plate basalts. The symbols are as in Fig. 7.

In Fig. 16 an internally consistent tectonic model for the evolution of the Qimantagh area with regard to Early Paleozoic is represented, and takes into account the results of recent geochronological data within the Qimantagh area as well as the data in this paper. Three main stages from subduction to *syn*-collision to post-collision extensional environments are recognized:

(1) Subduction (508–~430 Ma; Mo et al., 2007; Cui et al., 2011; Li et al., 2013; Wang et al., 2014; Meng et al., 2015; and references therein).
As a part of Proto-Tethys Ocean, the Qimantagh ocean might have formed in Early Cambrian (Mo et al., 2007; Meng et al., 2015; and references therein). Subsequently, northward subduction of the NEKT towards the QT was initiated during

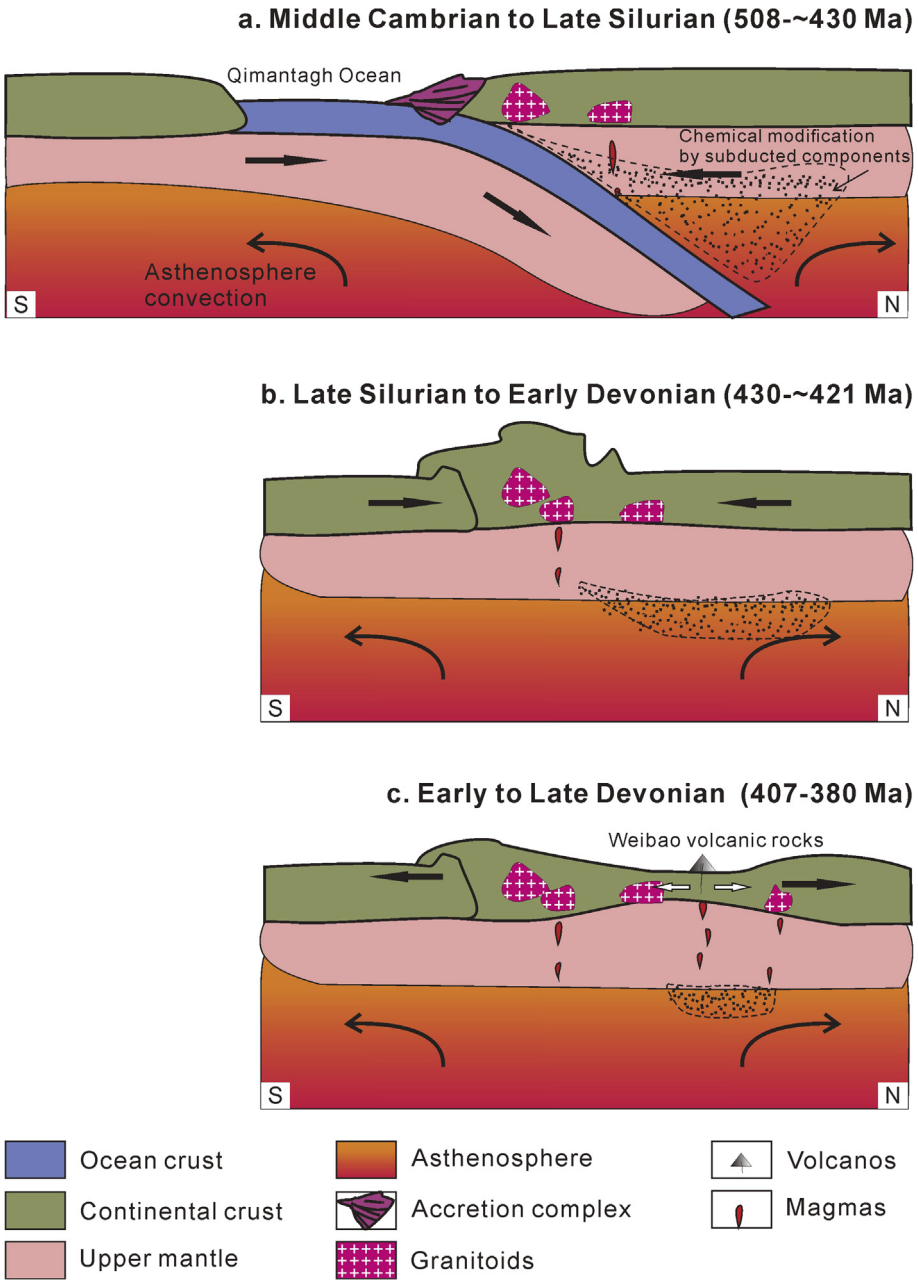

Fig. 16. Schematic cross-sections of the tectonic evolution of the Qimantagh area highlighting the genesis of the volcanic rocks within the Weibao deposit. Sections are roughly drawn in a south–north direction (present day coordinates).

Middle Cambrian to Early Ordovician (508–480 Ma) (Mo et al., 2007; Cui et al., 2011; Li et al., 2013), forming Heishan mafic–ultramafic complex (486 Ma; Meng et al., 2015) and Yaziquan diorite (480 Ma; Cui et al., 2011), as well as massive mafic and intermediate volcanic rocks (Sun et al., 2012; Zhang et al., 2015). This subduction was almost simultaneous with that in North Qilian (Mo et al., 2007; Xiao et al., 2009; and references therein). During subduction, the melts derived from subducted sediments and fluids rising from the sinking slab with remarkable enrichment of LILE relative to HFSE and relatively low zircon Hf isotopes gave rise to chemical modification of the overlying mantle. Consequently, the asthenospheric mantle above the subducted slab, which was thought to become the main source of the Weibao volcanic rocks in the later evolution progress, showed significant increases in LILE, e.g., Rb, Ba and LREE, as well as slightly enriched εHf values.

(2) syn-collision (430–~421 Ma; Cao et al., 2011; Liu et al., 2012; Wu et al., 2012; Hao et al., 2015).
Northward subduction ended up with the closure of the Qimantagh ocean and then the NEKT was welded to the QT at ca. 430 Ma, manifested by the occurrence of *syn*-collision granitoids from 430.8 Ma to 428.5 Ma (Cao et al., 2011; Wu et al., 2012), as well as deposition of molasses sediments of the Maoniushan Formation (ca. 423–400 Ma; Lu et al., 2010; Zhang et al., 2010). The igneous activity during this stage is relatively weak, and the resulting problem is that the time span of this stage is difficult to identify

precisely. But coeval high-K calc-alkaline I- and S-type granitoids with ages of ~421 Ma in the Qimantagh area suggested that the main *syn*-collision stage might have ceased since ~421 Ma (Hao et al., 2014).

(3) Post-collision (407–~380 Ma; Liu et al., 2012; Wang et al., 2014; Hao et al., 2015; and this study).
Large scale post-collision intrusions were mainly emplaced within a relatively narrow time span between 407 Ma and ca. 380 Ma in the Qimantagh region (Liu et al., 2012; Hao et al., 2015), although extension related to post-collision might have been triggered at ~419 Ma in the east of the EKOB (Yan et al., 2016). The extension was most probably triggered by gravitational collapse and spreading of the thickened and unstable lithosphere (see also Aldanmaz et al., 2000; Bonin, 2004). Although a continuous convecting within the asthenosphere will partly erase the enriched features that originated from influx of arc fluids and hydrous melts, volcanic arc-like features induced by the latest subduction could still survive. During extension, basaltic magmas derived from this modified depleted mantle source rose and erupted to the surface eventually, forming the Weibao volcanic rocks. Noticeably, contamination from the continental crust was negligible, but fractional crystallization was strongly manifested in those volcanic rocks. The melting might be induced by the upwelling and underplating of asthenospheric mantle. But obviously, this localized modified source region can melt more easily compared with the unenriched part as volatile components (H_2O and CO_2) in the mantle can lower the solidus of peridotite (e.g., Aldanmaz et al., 2000 and references therein). Finally, a post-orogenic molasses sequence, i.e., the Late Devonian Maoniushan Formation, marks the end of the Early Paleozoic–Middle Devonian orogenic cycle in this region, although the time span of the Maoniushan Formation is still controversial (Lu et al., 2013; Hao et al., 2014).

The combined petrologic-tectonic interpretation, proposed by Hao et al. (2015), for the evolution history within the Qimantagh area during Early Paleozoic is comparable in many respects to the above model. The crucial feature of our model, however, is that we emphasize that the compositions of the mantle-source regions forming the primary magmas of the Weibao volcanic rocks were modified by introduction of materials, in particular water and LILE, from an earlier subduction event. In other words, our research firmly demonstrate that magma types associated with subduction can, in some circumstances, be produced in areas where subduction is not contemporaneous with volcanism, as discovered in Papua New Guinea (Johnson et al., 1978). However, the extent and nature of this chemical modification are expected to have varied within the Weibao deposit, which might lead to variable degrees of enrichment and depletion of LILE and HFSE, such as Ba, Sr, Nb and Ta (Fig. 9).

6. Conclusions

We present geochronological and geochemical data for the new discovered lavas within the Weibao deposit. SHRIMP U–Pb zircon ages obtained from two samples are nearly consistent and indicate that the basaltic lavas erupted in Middle Devonian. Compositionally, these volcanic rocks are especially characterized by selective enrichment of LILE relative to HFSE and scattered zircon εHf(T) ratios, suggesting a mixed provenance involving combined asthenospheric mantle and fluids/melts inherited from an early subduction event. Additionally, the major and trace element systematics support a hornblende-dominated fractionation process during ascent of parental magmas. These results, together with previously published age data in the EKOB, firmly support that volcanic rocks within the Weibao deposit formed by post-collisional extension during Early to Middle Devonian.

Acknowledgements

This study was financially supported by the National Key Research and Development Plan (2016YFC0600205); the National Key Basic Research Program (Grant 2012CB416704) of the Ministry of Science and Technology, China; the Program of High-level Geological Talents (201309) and Youth Geological Talents (201112) of the China Geological Survey; grant No. 40772063 from the National Natural Science Foundation of China; and the IGCP-592 project sponsored by IUGS-UNESCO. We appreciate the assistance of Dr. Jiannan Liu, Miao Yu, Hui Wang and Jianhou Zhou from the CAGS during the fieldwork. We also thank Dr. Cailai Wu and Min Lei, Wei Zhang and other works from the CAGS for their assistance during the analyses. The Editor-in-Chief, Professor Franco Pirajno and two anonymous reviewers are especially thanked for their helpful input to improve the manuscript.

References

Aldanmaz, E., Pearce, J.A., Thirlwall, M., Mitchell, J., 2000. Petrogenetic evolution of late Cenozoic, post-collision volcanism in western Anatolia, Turkey. J. Volcanol. Geoth. Res. 102, 67–95.

Bonin, B., 2004. Do coeval mafic and felsic magmas in post-collisional to within-plate regimes necessarily imply two contrasting, mantle and crustal, sources? A review. Lithos 78, 1–24.

Bouvier, A., Vervoort, J.D., Patchett, P.J., 2008. The Lu–Hf and Sm–Nd isotopic composition of CHUR: constraints from unequilibrated chondrites and implications for the bulk composition of terrestrial planets. Earth Planet. Sci. Lett. 273, 48–57.

Cao, S.T., Liu, X.K., Ma, Y.S., Liu, J.Y., Ma, Y.L., 2011. The discovery and significance of early Silurian intrusions in the Qimantagh area. Qinghai Sci. Technol. 5, 26–30 (in Chinese with English abstract).

Cervantes, P., Wallace, P.J., 2003. Role of H2O in subduction-zone magmatism: new insights from melt inclusions in high-Mg basalts from central Mexico. Geology 31, 235–238.

Chen, H.W., Luo, Z.H., Mo, X.X., Zhang, X.T., Jin, W., Wang, B.Z., 2006. SHRIMP ages of Kayakedengtage complex in the East Kunlun Mountains and their geological implications. Acta Petrol. Mineral. 25, 25–32 (in Chinese with English abstract).

Chen, N.S., Xia, X.P., Li, X.Y., Sun, M., Xu, X.P., Liu, X.M., Wang, X.Y., Wang, Q.Y., 2007. Timing of magmatism of the gneissic-granite plutons along north Qaidam margin and implications for Precambrian crustal accretions: zircon U-Pb dating and Hf isotope evidence. Acta Petrol. Sin. 23, 501–512 (in Chinese with English abstract).

Cherniak, D., Watson, E., 2001. Pb diffusion in zircon. Chem. Geol. 172, 5–24.

Coleman, D.S., Gray, W., Glazner, A.F., 2004. Rethinking the emplacement and evolution of zoned plutons: geochronologic evidence for incremental assembly of the Tuolumne Intrusive Suite, California. Geology 32, 433–436.

Compston, W., Williams, I., Kirschvink, J., Zichao, Z., Guogan, M., 1992. Zircon U-Pb ages for the Early Cambrian time-scale. J. Geol. Soc. 149, 171–184.

Couzinié, S., Laurent, O., Moyen, J.F., Zeh, A., Bouilhol, P., Villaros, A., 2016. Post-collisional magmatism: crustal growth not identified by zircon Hf–O isotopes. Earth Planet. Sci. Lett. 456, 182–195.

Cui, M.H., Meng, F.C., Wu, X.K., 2011. Early Ordovician island arc of Qimantag Mountain, eastern Kunlun: evidence from geochemistry, Sm–Nd isotope and geochronology of intermediate-basic igneous rocks. Acta Petrol. Sin. 27, 3365–3379 (in Chinese with English abstract).

Fang, J., Chen, H.Y., Zhang, L., Zheng, Y., Li, D.F., Wang, C.M., Shen, D.L., 2015. Ore genesis of the Weibao lead–zinc district, Eastern Kunlun Orogen, China: constrains from ore geology, fluid inclusion and isotope geochemistry. Int. J. Earth Sci. 104, 1209–1233.

Feng, C.Y., Li, D.S., Qu, W.J., Du, A.D., Wang, S., Su, B.S., Jiang, J.H., 2009. Re–Os isotopic dating of molydenite from the Suolajier skarn-type copper–molybdenum deposit of Qimantage Mountain in Qinghai province and its geological significance. Rock Miner. Anal. 28, 223–227 (in Chinese with English abstract).

Feng, C.Y., Li, D.S., Wu, Z.S., Li, H.J., Zhang, Z.Y., Zhang, A.K., Shu, X.F., Su, S.S., 2010. Major types. time-space distribution and metallogeneses of polymetallic deposits in the Qimangtage metallogenic belt, Eastern Kunlun area. Northwestern Geol. 43, 10–17 (in Chinese with English abstract).

Feng, C.Y., Wang, X.P., Shu, X.F., Zhang, A.K., Xiao, Y., Liu, J.N., Ma, S.C., Li, G.C., Li, D. X., 2011a. Isotopic chronology of the Hutouya skarn lead–zinc polymetallic ore district in Qimantage area of Qinghai province and its geological significance. J. Jilin Univ. (Earth Science Edition) 41, 1806–1817 (in Chinese with English abstract).

Feng, C.Y., Zhao, Y.M., Li, D.X., Liu, J.N., Xiao, Y., Li, G.C., Ma, S.C., 2011b. Skarn types and mineralogical characteristics of the Fe–Cu–polymetallic Skarn deposits in the Qimantage area, western Qinghai Province. Acta Geol. Sin. (in Chinese with English abstract) 85, 1108–1115.
Feng, C.Y., Wang, S., Li, G.C., Ma, S.C., Li, D.S., 2012. Middle to Late Triassic granitoids in the Qimantage area, Qinghai Province, China: chronology, geochemistry and metallogenic significances. Acta Petrol. Sin. 28, 665–678 (in Chinese with English abstract).
Flowers, R., Bowring, S., Tulloch, A., Klepeis, K., 2005. Tempo of burial and exhumation within the deep roots of a magmatic arc, Fiordland, New Zealand. Geology 33, 17–20.
Gao, Y.B., Li, W.Y., 2011. Petrogenesis of granites containing tungsten and tin ores in the Baigahu deposit, Qimantage, NW China: constraints from petrology, chronology and geochemistry. Geochemica 40, 324–336 (in Chinese with English abstract).
Gao, Y.B., Li, W.Y., Tan, W.J., 2010. Metallogenic characteristics and analysis of the prospecting potential in the area of Qimantage. Northwestern Geol. 43, 35–43 (in Chinese with English abstract).
Gao, Y.B., Li, W.Y., Li, K., Qian, B., Zhang, Z.W., Zhou, A.S., Wu, Y.S., Zhang, J.W., Guo, Z.P., Wang, Y.L., 2012a. Genesis and chronology of Baiganhu-Jialesai W-Sn Mineralization Belt, Qimantage, East Kunlun Mountain, NW China. Northwestern Geol. 45, 229–241 (in Chinese with English abstract).
Gao, Y.B., Li, W.Y., Ma, X.G., Zhang, Z.W., Tang, Q.Y., 2012b. Genesis, geochronology and Hf isotopic compositions of the magmatic rocks in Galinge iron deposit, eastern Kunlun. J. Lanzhou Univ. (Nat. Sci.) 48, 36–47 (in Chinese with English abstract).
Gao, Y.B., Li, W.Y., Li, Z.M., Wang, J., Hattori, K., Zhang, Z.W., Geng, J.Z., 2014a. Geology, geochemistry, and genesis of tungsten–tin deposits in the Baiganhu district, northern Kunlun Belt, Northwestern China. Econ. Geol. 109, 1787–1799.
Gao, Y.B., Li, W.Y., Qian, B., Li, K., Li, D.S., He, S.Y., Zhang, Z.W., Zhang, J.W., 2014b. Geochronology, geochemistry and Hf isotopic compositions of the granitic rocks related with iron mineralization in Yemaquan deposit, East Kunlun, NW China. Acta Petrol. Sin. 30, 1647–1665 (in Chinese with English abstract).
Gao, Y.B., Li, W.Y., Qian, B., Li, K., Zhang, Z.W., Jiang, Z.X., Shen, D.L., Wang, Z.H., Ye, M.F., 2014c. Geology, fluid incluisions and S, Pb isotopic geochemistry of the Weibao Zn–Pb deposit in Qimantage, Xinjiang. J. Jilin Univ. (Earth Science Edition) (in Chinese with English abstract) 44, 1153–1165 (in Chinese with English abstract).
Gasparon, M., Varne, R., 1998. Crustal assimilation versus subducted sediment input in west Sunda arc volcanics: an evaluation. Mineral. Petrol. 64, 89–117.
Gorton, M.P., Schandl, E.S., 2000. From continents to island arcs: a geochemical index of tectonic setting for arc-related and within-plate felsic to intermediate volcanic rocks. Can. Mineral. 38, 1065–1073.
Griffin, W., Pearson, N., Belousova, E., Jackson, S., Van Achterbergh, E., O'Reilly, S.Y., Shee, S., 2000. The Hf isotope composition of cratonic mantle: LAM–MC–ICPMS analysis of zircon megacrysts in kimberlites. Geochim. Cosmochim. Acta 64, 133–147.
Hao, N.N., Yuan, W.M., Zhang, A.K., Cao, J.H., Chen, X.N., Feng, Y.L., Li, X., 2014. Late Silurian to Early Devonian Granitoids in the Qimantage area, East Kunlun Mountains: LA–ICP–MS zircon U-Pb ages, geochemical features and geological setting. Geol. Rev. 60, 201–215.
Hao, N.N., Yuan, W.M., Zhang, A.K., Feng, Y.L., Cao, J.H., Chen, X.N., Cheng, X.Q., Mo, X.X., 2015. Evolution process of the Late Silurian-Late Devonian tectonic environment in Qimantagh in the western portion of east Kunlun, China: evidence from the geochronology and geochemistry of granitoids. J. Earth Syst. Sci. 124, 171–196.
Hourigan, J., Solov'Ev, A., Ledneva, G., Garver, J., Brandon, M., Reiners, P., 2004. Timing of syenite intrusions on the eastern slope of the Sredinnyi Range, Kamchatka: rate of accretionary structure exhumation. Geochem. Int. 42, 97–105.
Jiang, Y.H., Jiang, S.Y., Dai, B.Z., Liao, S.Y., Zhao, K.D., Ling, H.F., 2009. Middle to late Jurassic felsic and mafic magmatism in southern Hunan province, southeast China: implications for a continental arc to rifting. Lithos 107, 185–204.
Johnson, R., Mackenzie, D., Smith, I., 1978. Delayed partial melting of subduction-modified mantle in Papua New Guinea. Tectonophysics 46, 197–216.
Lambert, R.S.J., Holland, J.G., Owen, P.F., 1974. Chemical petrology of a suite of calc-alkaline lavas from Mount Ararat, Turkey. J. Geol., 419–438
Le Bas, M.J., Le Maitre, R., Streckeisen, A., Zanettin, B., 1986. A chemical classification of volcanic rocks based on the total alkali-silica diagram. J. Petrol. 27, 745–750.
Lee, J.K., Williams, I.S., Ellis, D.J., 1997. Pb, U and Th diffusion in natural zircon. Nature 390, 159–162.
Li, W.Y., 2010. The geological composition and metallogenetic prospect in the Qimantage prospective region, East Kunlun. Northwestern Geol. 43, 1–9 (in Chinese with English abstract).
Li, F., Wu, Z.L., Li, B.Z., 2007. Recognition on formation age of the tanjianshan group on the northern margin of the Qaidam basain and its geological significance. Geotectonica et Metallogenia 31, 226–233 (in Chinese with English abstract).
Li, S.J., Sun, F.Y., Feng, C.Y., Liu, Z.Y., Zhao, J.W., Li, Y.C., Wang, S., 2008. Geochronological Study on Yazigou Polymetallic Deposit in Eastern Kunlun, Qinhai Province. Acta Geol. Sin. 82, 949–955 (in Chinese with English abstract).
Li, G.C., Feng, C.Y., Wang, R.J., Ma, S.C., Li, H.M., Zhou, A.S., 2012. SIMS zircon U-Pb age, petrochemistry and tectonic implications of granitoids in northeastern Baiganhu W–Sn orefield, Xinjiang. Acta Geosci. Sin. 33, 216–226 (in Chinese with English abstract).
Li, W., Neubauer, F., Liu, Y.J., Genser, J., Ren, S.M., Han, G.Q., Liang, C.Y., 2013. Paleozoic evolution of the Qimantagh magmatic arcs, Eastern Kunlun Mountains: constraints from zircon dating of granitoids and modern river sands. J. Asian Earth Sci. 77, 183–202.
Li, R.B., Pei, X.Z., Li, Z.C., Pei, L., Liu, C.J., Chen, Y.X., Chen, G.C., Liu, Z.Q., Yang, J., 2015. Geochemistry and zircon U-Pb geochronology of granitic rocks in the Buqingshan tectonic mélange belt, northern Tibet Plateau, China and its implications for Prototethyan evolution. J. Asian Earth Sci. 105, 374–389.
Liu, F.L., Xu, Z.Q., Liou, J.G., Song, B., 2004. SHRIMP U-Pb ages of ultrahigh-pressure and retrograde metamorphism of gneisses, south–western Sulu terrane, eastern China. J. Metamorph. Geol. 22, 315–326.
Liu, Y.J., Genser, J., Neubauer, F., Jin, W., Ge, X.H., Handler, R., Takasu, A., 2005. 40 Ar/39 Ar mineral ages from basement rocks in the Eastern Kunlun Mountains, NW China, and their tectonic implications. Tectonophysics 398, 199–224.
Liu, B., Ma, C.Q., Zhang, J.Y., Xiong, F.H., Huang, J., Jiang, H.A., 2012. Petrogenesis of Early Devonian intrusive rocks in the east part of Eastern Kunlun Orogen and implication for Early Palaeozoic orogenic processes. Acta Petrol. Sin. 28, 1785–1807 (in Chinese with English abstract).
Liu, B., Ma, C.Q., Guo, P., Zhang, J.Y., Xiong, F.H., Huang, J., Jiang, H.A., 2013. Discovery of the Middle Devonian A-type granite from the Eastern Kunlun Orogen and its tectonic implications. Earth Sci.-J. China Univ. Geosci. 38, 947–962.
Liu, T., Zhai, Q.G., Wang, J., Bao, P.S., Qiangba, Z., Tang, S.H., Tang, Y., 2016. Tectonic significance of the Dongqiao ophiolite in the north–central Tibetan plateau: evidence from zircon dating, petrological, geochemical and Sr–Nd–Hf isotopic characterization. J. Asian Earth Sci. 116, 139–154.
Lu, L., Wu, Z.H., Hu, D.G., Barosh, P.J., Hao, S., Zhou, C.J., 2010. Zircon U-Pb age for rhyolite of the Maoniushan Formation and its tectonic significance in the East Kunlun Mountains. Acta Petrol. Sin. 26, 1150–1158 (in Chinese with English abstract).
Lu, L., Zhang, Y.L., Wu, Z.H., Hu, D.G., 2013. Zircon U-Pb Dating of Early Paleozoic Granites from the East Kunlun Mountains and its geological significance. Acta Geol. Sin. 34, 447–454.
Lugwig, K., 2001. Squid 1.02: A User's Manual. Berkeley Geochronology Center Special Publication, 15–35.
Luo, Z.H., Ke, S., Cao, Y.Q., Deng, J.F., Chen, H.W., 2002. Late Indosinian mantle-derived magmatism in the East Kunlun. Geol. Bull. China 21, 292–297.
Manikyamba, C., Kerrich, R., Khanna, T.C., Satyanarayanan, M., Krishna, A.K., 2009. Enriched and depleted arc basalts, with Mg-andesites and adakites: a potential paired arc–back-arc of the 2.6 Ga Hutti greenstone terrane, India. Geochim. Cosmochim. Acta 73, 1711–1736.
Mazzeo, F., D'Antonio, M., Arienzo, I., Aulinas, M., Di Renzo, V., Gimeno, D., 2014. Subduction-related enrichment of the Neapolitan volcanoes (Southern Italy) mantle source: new constraints on the characteristics of the slab-derived components. Chem. Geol. 386, 165–183.
Meng, F.C., Cui, M.H., Wu, X.K., Ren, Y.F., 2015. Heishan mafic–ultramafic rocks in the Qimantag area of Eastern Kunlun, NW China: remnants of an early Paleozoic incipient island arc. Gondwana Res. 27, 745–759.
Mo, X.X., Luo, Z.H., Deng, J.F., Yu, X.H., Liu, C.D., Chen, H.W., Yuan, W.M., Liu, Y.H., 2007. Granitoids and crustal growth in the East-Kunlun Orogenic Belt. Geol. J. China Univ. 13, 403–414 (in Chinese with English abstract).
Notsu, K., Fujitani, T., Ui, T., Matsuda, J., Ercan, T., 1995. Geochemical features of collision-related volcanic rocks in central and eastern Anatolia, Turkey. J. Volcanol. Geoth. Res. 64, 171–191.
Pearce, J.A., 1982. Trace element characteristics of lavas from destructive plate boundaries. Andesites 8, 525–548.
Pearce, J.A., 1996. A user's guide to basalt discrimination diagrams. Trace element geochemistry of volcanic rocks: applications for massive sulphide exploration. Geological Association of Canada, Short Course. Notes 12, 113.
Pearce, J.A., Norry, M.J., 1979. Petrogenetic implications of Ti, Zr, Y, and Nb variations in volcanic rocks. Contrib. Miner. Petrol. 69, 33–47.
Pearce, J.A., Peate, D.W., 1995. Tectonic implications of the composition of volcanic arc magmas. Annu. Rev. Earth Planet. Sci. 23, 251–286.
Pearce, J.A., Bender, J., De Long, S., Kidd, W., Low, P., Güner, Y., Saroglu, F., Yilmaz, Y., Moorbath, S., Mitchell, J., 1990. Genesis of collision volcanism in Eastern Anatolia, Turkey. J. Volcanol. Geoth. Res. 44, 189–229.
Peccerillo, A., 1998. Relationships between ultrapotassic and carbonate-rich volcanic rocks in central Italy: petrogenetic and geodynamic implications. Lithos 43, 267–279.
Polat, A., Kerrich, R., 2002. Nd-isotope systematics of∼ 2.7 Ga adakites, magnesian andesites, and arc basalts, Superior Province: evidence for shallow crustal recycling at Archean subduction zones. Earth Planet. Sci. Lett. 202, 345–360.
Söderlund, U., Patchett, P.J., Vervoort, J.D., Isachsen, C.E., 2004. The ^{176}Lu decay constant determined by Lu–Hf and U-Pb isotope systematics of Precambrian mafic intrusions. Earth Planet. Sci. Lett. 219, 311–324.
Squire, R., Wilson, C., Dugdale, L., Jupp, B., Kaufman, A., 2006. Cambrian backarc-basin basalt in western Victoria related to evolution of a continent-dipping subduction zone. Aust. J. Earth Sci. 53, 707–719.
Sun, S.S., McDonough, W.F., 1989. Chemical and isotopic systematics of oceanic basalts: implications for mantle composition and processes. Geological Society, London, Special Publications 42, 313–345.
Sun, H.S., Zhan, L.J., Wu, G.B., Ning, J.T., Chen, Q.M., Jiang, C.L., 2012. Metallogenic tectonic setting and ore-finding potential of Xitieshan massive sulfide lead–zinc deposit: evidence from lithochemistry and geochemistry of ore-hosted volcanic strata, Tanjianshan Group. Acta Petrol. Sin. 28, 652–664 (in Chinese with English abstract).

Vavra, G., Gebauer, D., Schmid, R., Compston, W., 1996. Multiple zircon growth and recrystallization during polyphase Late Carboniferous to Triassic metamorphism in granulites of the Ivrea Zone (Southern Alps): an ion microprobe (SHRIMP) study. Contrib. Miner. Petrol. 122, 337–358.
Wan, Y.S., Song, B., Liu, D.Y., Wilde, S.A., Wu, J.S., Shi, Y.R., Yin, X.Y., Zhou, H.Y., 2006. SHRIMP U-Pb zircon geochronology of Palaeoproterozoic metasedimentary rocks in the North China Craton: evidence for a major Late Palaeoproterozoic tectonothermal event. Precambr. Res. 149, 249–271.
Wang, H.C., Wu, S.N., Yuan, G.B., Xin, H.T., Zhang, B.H., Wang, Q.H., Tan, Q., 2003. Tectonic setting and age of the "Tanjianshan Group" on the northern margin of the Qaidam basin. Geol. Bull. China 22, 487–493 (in Chinese with English abstract).
Wang, S., Feng, C.Y., Li, S.J., Jiang, J.H., Li, D.S., Su, B.S., 2009. Zircon SHRIMP U-Pb dating of granodiorite in the Kaerqueka polymetallic ore deposit, Qimantage Mountain, Qinghai Province, and its geological implications. Geol. China 36, 74–84.
Wang, G., Sun, F.Y., Li, B.L., Li, S.J., Zhao, J.W., Yang, Q., Ao, Z., 2013. Zircon U-Pb Geochronology and Geochemistry of the Early Devonian Syenogranite in the Xiarihamu Ore District from East Kunlun, with Implications for the Geodynamic Setting. Geotectonica et Metallogenia 37, 685–697 (in Chinese with English abstract).
Wang, Z.Z., Han, B.F., Feng, C.Y., Li, G.C., 2014. Geocheronology, geochemistry and tectonic significance of granites in Baiganhu area, Xinjiang. Acta Petrol. Mineral. 33, 597–616 (in Chinese with English abstract).
Wang, X.C., Wilde, S.A., Xu, B., Pang, C.J., 2016. Origin of arc-like continental basalts: implications for deep-Earth fluid cycling and tectonic discrimination. Lithos. http://dx.doi.org/10.1016/j.lithos.2015.12.014.
Watchorn, R., Wilson, C., 1989. Structural setting of the gold mineralisation at Stawell, Victoria, Australia. Econ. Geol. Monogr. 6, 292–309.
Weaver, B.L., 1991. Trace element evidence for the origin of ocean-island basalts. Geology 19, 123–126.
Winkler, H., 1957. Experimentelle Gesteinsmetamorphose—I Hydrothermale Metamorphose karbonatfreier Tone. Geochim. Cosmochim. Acta 13, 42–69.
Wood, D.A., 1980. The application of a Th Hf Ta diagram to problems of tectonomagmatic classification and to establishing the nature of crustal contamination of basaltic lavas of the British Tertiary Volcanic Province. Earth Planet. Sci. Lett. 50, 11–30.
Wu, F.Y., Yang, Y.H., Xie, L.W., Yang, J.H., Xu, P., 2006. Hf isotopic compositions of the standard zircons and baddeleyites used in U-Pb geochronology. Chem. Geol. 234, 105–126.
Wu, S.F., Chen, L.B., Ren, W.K., Zhang, H.Q., Wang, S.H., Ding, C.W., 2012. Discovery of rapakivite grantite and its geological implication in Qimantage. J. Qinghai Univ. (Natural Science Edition) 30, 49–54 (in Chinese with English abstract).
Xia, L.Q., 2014. The geochemical criteria to distinguish continental basalts from arc related ones. Earth Sci. Rev. 139, 195–212.
Xiao, W.J., Windley, B.F., Yong, Y., Yan, Z., Yuan, C., Liu, C.Z., Li, J.L., 2009. Early Paleozoic to Devonian multiple-accretionary model for the Qilian Shan, NW China. J. Asian Earth Sci. 35, 323–333.
Xiao, Y., Feng, C.Y., Liu, J.N., Yu, M., Zhou, J.H., Li, D.X., Zhao, Y.M., 2013. LA–MC–ICP–MS zircon U-Pb dating and sulfur isotope characteristics of Kendekeke Fe-polymetallic deposit, Qinghai Province. Miner. Deposits 32, 177–186 (in Chinese with English abstract).
Xiong, F.H., Ma, C.Q., Zhang, J.Y., Liu, B., 2012. The origin of mafic microgranular enclaves and their host granodiorites from East Kunlun, Northern Qinghai-Tibet Plateau: implications for magma mixing during subduction of Paleo-Tethyan lithosphere. Mineral. Petrol. 104, 211–224.
Xiong, F.H., Ma, C.Q., Jiang, H.A., Liu, B., Huang, J., 2014. Geochronology and geochemistry of Middle Devonian mafic dykes in the East Kunlun orogenic belt, Northern Tibet Plateau: implications for the transition from Prototethys to Paleotethys orogeny. Chem. Erde 74, 225–235.
Xiong, F.H., Ma, C.Q., Wu, L., Jiang, H.A., Liu, B., 2015. Geochemistry, zircon U-Pb ages and Sr–Nd–Hf isotopes of an Ordovician appinitic pluton in the East Kunlun orogen: new evidence for Proto-Tethyan subduction. J. Asian Earth Sci. 111, 681–697.
Xu, C.K., Liu, S.B., Zhao, Z.J., Zhang, M.F., Zhang, K.C., Liu, J.H., Zhan, Y.F., Huang, C.H., Zhang, Z.Y., Wang, H.Y., Zhang, W.J., Qiao, Q., 2012. Metallogenic law and prospect direction of iron deposits in the east Kunlun metallogenic belt in Qinghai. Acta Geol. Sin. 86, 1621–1678 (in Chinese with English abstract).
Yan, W., Qiu, D.M., Ding, Q.F., Liu, F., 2016. Geochronology, Petrogenesis, source and its structural significance of Houtouya Monzogranite of Wulonggou area in Eastern Kunlun Orogen. J. Jilin Univ. (Earth Science Edition) 46, 443–460 (in Chinese with English abstract).
Yang, J.S., Robinson, P., Jiang, C.F., Xu, Z.Q., 1996. Ophiolites of the Kunlun Mountains, China and their tectonic implications. Tectonophysics 258, 215–231.
Yu, M., Feng, C.Y., Liu, H.C., Li, D.W., Zhao, Y.M., Li, D.X., Liu, J.N., Wang, H., Zhang, M. H., 2015. 40Ar–39Ar geochronology of the Galinge large skarn iron deposit in Qinghai province and geological significance. Acta Geol. Sin. 89, 510–521 (in Chinese with English abstract).
Zhang, Y., Hu, D., Shi, Y., Lu, L., 2010. SHIRMP zircon U-Pb ages and tectonic significance of Maoniushan Formation volcanic rocks in East Kunlun orogenic belt, China. Geol. Bull. China 29, 1614–1618 (in Chinese with English abstract).
Zhang, J.Y., Ma, C.Q., Xiong, F.H., Liu, B., Li, J.W., Pan, Y.M., 2014. Early Paleozoic high-Mg diorite-granodiorite in the eastern Kunlun Orogen, western China: response to continental collision and slab break-off. Lithos 210, 129–146.
Zhang, X.P., Wang, Q.F., Hui, J., Chang, X., Tong, H.K., 2015. Chmical characteristics of volcanic rocks from the Tanjianshan Group on the northern margin of the Qaidam basin and its tectonic environment. J. Miner. Petrol 35, 18–26 (in Chinese with English abstract).
Zhao, Y.M., Feng, C.Y., Li, D.X., Liu, J.N., Xiao, Y., Yu, M., Ma, S.C., 2013. Metallogenic setting and mineralization-alteration characteristics of major skarn Fe-polymetallic deposits in Qimantag area, western Qinghai Province. Miner. Deposits 32, 1–19 (in Chinese with English abstract).
Zhou, J.H., Feng, C.Y., Li, D., Wang, H., Zhang, M.Y., Li, G.C., Wang, Z.Z., 2015. Petrology, geochronology and geochemistry of metallogenetic granite in Baiganhu W-Sn deposit, East Kunlun. Acta Petrol. Sin. 31, 2277–2293 (in Chinese with English abstract).